Journal of Asian Earth Sciences 83 (2014) 13–34

Contents lists available at ScienceDirect

Journal of Asian Earth Sciences

journal homepage: www.elsevier.com/locate/jseaes

Petrography, mineralogy and geochemistry of Cretaceous sediment samples from western Khorat Plateau, Thailand, and considerations on their provenance

Seriwat Saminpanya [a,*], Jaroon Duangkrayom [b], Pratueng Jintasakul [b], Rattanaphorn Hanta [b]

[a] Department of General Science, Faculty of Science, Srinakharinwirot University, Bangkok 10110, Thailand
[b] Northeastern Research Institute of Petrified Wood & Mineral Resources (In Honour of His Majesty the King) Nakhon Ratchasima Rajabhat University, Nakhon Ratchasima, Thailand

ARTICLE INFO

Article history:
Received 30 June 2013
Received in revised form 19 December 2013
Accepted 5 January 2014
Available online 17 January 2014

Keywords:
Mineralogy
Geochemistry
Provenance
Khorat Group
Phra Wihan Formation
Chemical Index of Alteration
Mo Hin Khao

ABSTRACT

At Mo Hin Khao on the western flank of Khorat Plateau, Thailand, the Phra Wihan Formation reveals litharenite and sublitharenite with some subarkose and arkose. A cuesta in the eroded sedimentary sequence exhibits spectacular rock pillars of considerable geotourist potential. The rock sequence is high in silica (SiO_2 67–98 wt%) and contains quartz, mica, magnetite, chert fragments and accessory minerals such as zircon and tourmaline and amphibole species. These accessory minerals suggest felsic rocks, such as granite, granodiorite and pegmatite, were sources for the sandstones. Geochemical analyses of the sedimentary sequence suggest that source rocks may lie in the passive continental margin, before sediment transport and deposition in the Khorat Basin by rivers flowing across a large flood plain. Many depositional sequences/episodes formed thick beds of cross bedded clastic rocks. A high average maturity index (>5) indicates sedimentary reworking/recycling. Chemical Index of Alteration (CIA) values range from 47 to 98, suggesting variable chemical weathering within the source area rocks, largely representing moderate to high degrees of weathering. The average CIA value of these sediments (78) suggests that relatively extreme alteration factors were involved.

1. Introduction

The Mo Hin Khao cuesta on the western edge of the Khorat Plateau, formed by erosion of clastic rocks of the Phra Wihan Formation, within the Mesozoic Khorat Group (Fig. 1). The site is located within the Phulaenkha national forest in the Chaiyaphum province, Thailand and covers an area of 0.32 km^2 at an elevation of 800 m a.s.l. The dipslope (strike N–S with low-angle dip, <15°E) has a steep escarpment to the west. The Phra Wihan Formation was deposited in the early Cretaceous (Barriasian to Barremian, 125–145 Ma), on the basis of palynological data from near the base of the formation (Racey et al., 1996; Racey and Goodall, 2009). These light buff to gray, fine-grained to coarse-grained quartzitic sandstones and rarer siltstone and mudstone with occasional conglomerate were reported as deposits of braided and meandering streams in a tropical palaeoclimate (Meesook, 2000). Racey and Goodall (2009) interpreted them as deposits within a fluvial environment dominated by high-energy, shallow braided rivers with subordinate low energy meandering river systems and associated floodplains. Both the Phra Wihan and underlying Phu Kradang Formations have been interpreted as deposits of an anastomosing river system within a semi-arid to sub-humid paleoclimate with wet-dry cycles (Horiuchi et al., 2012). The contacts between the Phu Kradung and overlying Phra Wihan and Sao Khua Formations are all gradational and conformable. The high-frequency occurrence of *Corollina* (*Classopollis*) indicates an Early Cretaceous age for the Phra Wihan Formation with a warm climate, seasonally dry, and subtropical palaeoclimate for the area. The thickness is 100–250 m (Racey and Goodall, 2009; Meesook, 2011). Although the Phu Kradung Formation is also early Cretaceous, the lowest part could be Late Jurassic (Racey and Goodall, 2009); its thickness ranges from 800 m to 1200 m. The rocks are generally composed of maroon siltstone and claystone but sandstone and conglomerate are also found (Meesook and Saengsrichan, 2011). According to Racey (2009), the Phu Kradung Formation sits conformably on the Nam Phong Formation, which includes an upper member of Late Jurassic age, and a lower member of Late Triassic age, separated by a hiatus (Racey, 2009). That hiatus is adopted by some authors as the base of the Khorat Group (e.g. Racey, 2009; Booth and Sattayarak, 2011), whereas others (e.g. Meesook and Saengsrichan, 2011) place the base of the Khorat Group at the base of the lower Nam Phong Formation. The Phu Kradung Formation comprises red-brown micaceous sandstone, conglomerate, siltstone and mudstone of mainly fluviatile origin.

* Corresponding author. Tel.: +66 26495000x18668; fax: +66 26495628.
E-mail address: seriwat@hotmail.com (S. Saminpanya).

1367-9120/$ - see front matter © 2014 Elsevier Ltd. All rights reserved.
http://dx.doi.org/10.1016/j.jseaes.2014.01.007

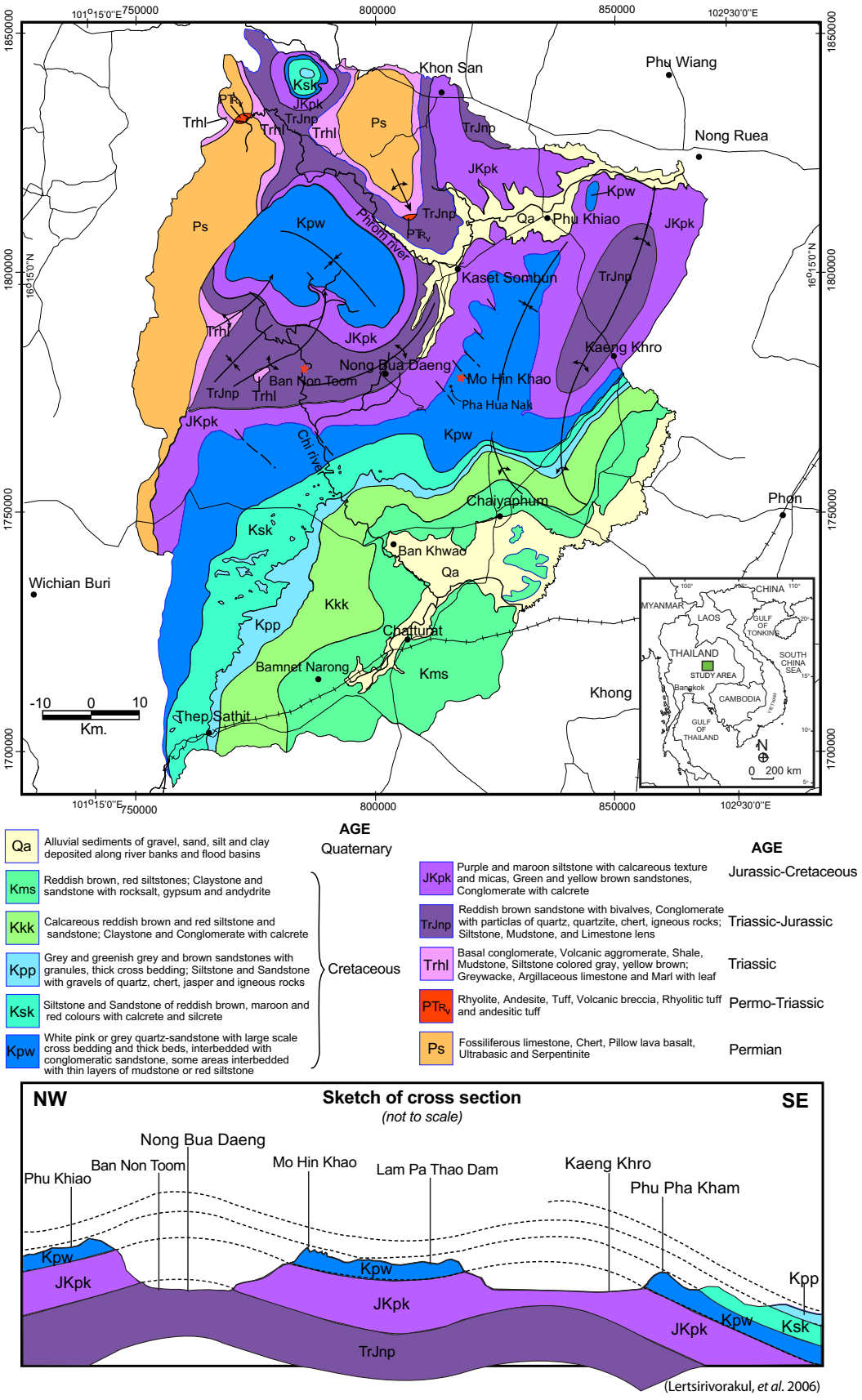

Fig. 1. Location and geological maps of Chaiyaphum province. (Rock boundaries are from Department of Mineral Resources (2007).) (See above-mentioned reference for further information.)

The sandstones in the Nam Phong Formation are medium and fine-grained and usually calcareous (Chonglakmani, 2011).

The dipslope of the Mo Hin Khao area supports over 300 pillars/hillocks which are the remnants of weathering and erosion of Phra Wihan sandstone. Five rock pillars, 9–12 m high and 3–5 m wide stand out and are reputedly the largest natural rock pillars in Southeast Asia. Therefore this area is a target for a sustainable geotourism and has been officially designated as a tourism site since 2009. Important fossils, e.g. dinosaur footprints and bones, have been discovered in 14 localities of Chaiyaphum; for example, the oldest known sauropods (*Isanosaurus attavipachi*) in the Late Triassic Nam Phong Formation (Buffetaut et al., 2000) and the first parrot-beak ceratopsian in Southeast Asia (*Psittacosaurus sattayaraki*) in the Early Cretaceous of Khok Kruat Formation (Buffetaut and Suteethorn, 1992). Due to their importance for science and tourism purposes, several development projects have been proposed by the governor; e.g., the Mo Hin Khao landscape development, the Upper Chi Valley Dinosaur Park and the Chaiyaphum Dinosaur Museum.

This study aims to improve understanding of the geological history of the Mo Hin Khao area. Although the Mesozoic lithostratigraphy is well documented (e.g. Sattayarak, 1985; Racey et al., 1996; Meesook, 2000, 2011; Meesook et al., 2002; Racey, 2009), the provenance and paleoenvironments are less certain. A provenance study in an adjacent area of Permian sediments (Malila et al., 2008) and detrital zircon U–Pb and fission track chronology (Carter and Bristow, 2003) investigated the Khorat Group sediment provenance. Although the latter provided some insights about the provenance of the zircons it did not characterize the sediments as a whole. To address this, we conducted a geochemical provenance study and used this to discuss the degree of chemical weathering of the souce area. In addition, comparative analyses of fossil-bearing clastic rocks of the Nam Phong Formation at Ban Non Toom (samples prefixed as BNT), Nong Bua Daeng district, ~30 km west of Mo Hin Khao (Fig. 1) are also given.

2. Methods

Samples (prefixed as MHK) were collected from rock beds on the dipslope and escarpment of the area for laboratory analysis and stratigraphic logging. Three out of five rock pillars were sampled by riding on a boom lift truck. Smaller, shorter rock pillars/hillocks on the dipslope were not sampled. Forty-one polished sections were made for petrographic study.

The mineral species of 14 powdered samples were first determined by an X-ray diffraction (XRD) technique. The major minerals and others unresolved by petrography were analyzed by Electron Probe Microanalysis (EPMA). Total oxides of all elements were in the range of 100 ± 1.5 wt%. The wt% of iron as $Fe_2O_{3(Total)}$, obtained by this technique was recalculated to the wt% of Fe_2O_3 and FeO through the equations of Droop (1987). The number of cations for each mineral cell formula is based on Deer et al. (1996) and Droop (1987). Geochemistry (major and trace elements) was analyzed by X-ray fluorescence (XRF). Loss on Ignition (LOI) of the samples was determined from the weight loss after roasting ~1.0 g powdered specimen at 1050 °C for 2 h.

The Chemical Index of Alteration (CIA) is used to assess the degree of chemical weathering (e.g. Nesbitt and Young, 1982; Rahman and Suzuki, 2007; Shao et al., 2012) and to characterize the palaeoclimate. The CIA index is calculated using the following equation: $CIA = [Al_2O_3/(Al_2O_3 + CaO^* + Na_2O + K_2O)] \times 100$ (molar proportions), where CaO^* represents the amount of CaO incorporated in the silicate phases (Fedo et al., 1995). The sediments that are enriched in non-silicate CaO (i.e. calcite-rich samples) are excluded from these calculations (Ghandour et al., 2003).

3. Results

3.1. Lithology

3.1.1. Lithology of the five rock pillars on the dipslope at Mo Hin Khao

The rocks are sandstone containing mainly quartz and some magnetite grains (Table 1). Grain sizes are medium to coarse with sub-rounded to sub-angular and moderately sorted to well-sorted fabric. There are sparse granules of quartz. Holes are common at the bottom surface of the beds. Based on their surface features and stratigraphy, all five rock pillars are similar and their beds can be correlated from one pillar to another, which allows the successions to be divided into four depositional sequences/layers from bottom to the top (Fig. 2), as follows:

(1) The bottom layer contains well-cemented matrix from the more resistant lower part to a less-cemented portion of the upper part. Grain size decreases upsection from coarse to medium sand. Cross-bedding is observed throughout.
(2) A layer of coarse sand, with granules, is fairly-well cemented, with cross-bedding throughout.
(3) The finest particle size forms this layer, with rare granules, mostly at the bottom. Smaller-scale cross sets occur throughout the layer. Grainsize fines upwards and the layer is well cemented.
(4) The top resistant layer consists of well-cemented coarse to very coarse-sand with widely disseminated granules and cross-bedding.

3.1.2. Lithology of the rocks at the escarpment of Mo Hin Khao area

These rocks lie downhill and to the west of the peak (at "Pha Hua Nak") (Table 2). An upper unit contains yellow-brown to white sandstone beds intercalated in places with green thinner sandstone beds. Cross-bedding is very common (Fig. 3a). This fine to medium sandstone is coarser in grain size on the dipslope, than in the escarpment sections. The minerals are mainly quartz with some mica and magnetite. The underlying Phu Kradung Formation (Fig. 3b) is characterized by red to maroon siltstone, reddish-purple mudstone, and gray to greenish-brown fine to medium grained sandstone. The rocks show spheroidal fracture and ripple marks. Quartz and mica are the major component.

3.2. Petrography

The rocks contain quartz (>90% in some samples) with accessory feldspar and lithic grains (3–5% each), muscovite (1–3%) and other minerals (<1%, amphibole, zircon, magnetite, tourmaline and clay minerals). Grains range from rounded to euhedral. Feldspars are mostly weathered to clay (kaolinite and illite) or secondary mica minerals (Fig. 4). The Q–F–L (Quartz–Feldspar–Lithic) diagram shows the Mo Hin Khao rocks fall mainly in the quartz arenite field; some are subarkose and sublitharenite (Fig. 5).

3.3. X-ray Diffraction (XRD) and Electron Probe Microanalysis (EPMA)

XRD, Table 3 shows the minerals found in the samples. EPMA analyses include quartz (four detrital grains and one micro quartz in chert fragment); muscovite (two); feldspar (five albites and one orthoclase); tourmaline (two); zircon (six); magnetite (two); amphibole (six); and clay mineral (two). The selected analyses are shown in Table 4.

Table 1
Lithological description of the 3 rock pillars at Mo Hin Khao area.

Depth (thickness) in cm	Sample	Description
Rock Pillar #1 ("Khun Sri Wichai"), UTM Grid 47Q 817432/1778276, Date: 29 March 2011		
1030–1220 (top) (190)	MHK-065, MHK-066	Yellowish brown, medium grained sandstone, well sorted, sub-round, quartz rich, magnetite rare, Fe-oxide, polygonal cracks on the top surface, trough cross-bedding
880–1030 (150)	MHK-067	White, medium-coarse grained sandstone with granules (light), moderately sorted, sub-angular to angular, quartz (yellow) rich, magnetite rare, clay clasts, sand nodules, erosional bottom surface contact, large scale planar cross-bedding
600–880 (280)	MHK-068, MHK-069	*Upper part*; White, medium grained sandstone, well sorted, sub-round to round, quartz rich, magnetite rare, sand nodules (light), high dip angles of cross-bedding = 30°SE, 24°SE and 14°E *Lower part*; White, medium grained sandstone with granules (rare), well sorted, sub-round, quartz rich, magnetite rare, sharp contact bottom surface, large scale planar cross-bedding, cross-bedding dip angles = 10°W, 9°W, 14°W, 10°W, 15°W and 10°W
525–600 (75)	MHK-070	White, fine-medium grained sandstone, well sorted, sub-angular to sub-round, quartz rich (pink), magnetite rare, sharp contact bottom surface, tabular cross-bedding, cross-bedding dip angles = 6°W, 4°W, 17°W, 14°W, 11°W, 19°W, 15°W and 4°W
365–525 (160)	MHK-071	White, medium-coarse grained sandstone with granules, poorly sorted, sub-angular to angular, quartz rich, magnetite rare, trough cross-bedding, erosional bottom surface contact with a lot of holes (trace of sand nodules) at the surface
310–365 (55)	MHK-072	Brownish white, fine-medium grained sandstone, well sorted, sub-angular, quartz rich (yellow), magnetite rare, Fe-oxide stained sand nodules, trough cross-bedding, bedding plane = strike N55W dip 15°E, erosional bottom surface, a lot of holes on the upper part
200–310 (110)	MHK-073	Brownish white, medium grained sandstone, moderately sorted, sub-angular, quartz rich, magnetite rare (prismatic habit), Fe-oxide of sand nodule (brown), trough cross-bedding, erosional bottom surface contact and a lot of holes (trace of sand and mud nodules)
(bottom) 0–200 (200)	MHK-074	Brownish white, medium-coarse grained sandstone, moderately sorted, sub-angular, quartz rich, magnetite rare, large scale planar cross-bedding
Rock Pillar #2 ("Pu Rue Si"), UTM Grid 47Q 817406/1778280, Date: 29 March 2011		
800–900 (top) (100)	MHK-057	Pinkish white, coarse-very coarse grained sandstone with granule, moderately sorted, sub-angular to sub-round, quartz rich, magnetite rare, Fe-oxide stained sand nodules, planar cross-bedding, erosional bottom surface contact, cross-bedding dip angle = E, polygonal cracks on the top surface
710–800 (90)	–	Pinkish white, coarse-very coarse grained sandstone with granule, moderately sorted, sub-angular to sub-round, quartz rich, magnetite rare, large scale planar cross-bedding, erosional bottom surface contact
525–710 (185)	MHK-058, MHK-059	Pinkish white, medium-coarse grained sandstone, moderately sorted, sub-angular to sub-round, quartz (pink) rich, magnetite rare, Fe-oxide of sand nodules, clay nodules, erosional bottom surface contact, trough cross-bedding with dip angles = 18°E, 14°E, 13°E, 13°E, 5°W, 2°W, 24°E, 18°E, 16°E, 15°E, 13°E and 6°E,
425–525 (100)	MHK-060	Brownish white, medium-coarse grained sandstone with granules, moderately sorted, sub-angular, quartz rich, sand nodules, planar cross-bedding, erosional bottom surface contact and contain a lot of holes (trace of sand nodules)
265–425 (160)	MHK-061, MHK-062	Brownish white, coarse grained sandstone with granules, moderately sorted, sub-angular, quartz rich (at surface = pink and yellow quartz grains), 5% magnetite (hexagonal prism habit), sand nodules, a lot of holes (trace of sand and mud nodules) in the lower part, large scale planar cross-bedding with high dip angle = 45°E
(bottom) 0–265 (265)	MHK-063, MHK-064	*Upper part*; Brownish white, medium grained sandstone, moderately sorted, sub-angular, quartz rich, magnetite rare, bottom surface contact contain a lot of holes (trace of sand and mud nodules) *Lower part*; Brownish white, coarse-very coarse grained sandstone with granules, fining upward, poorly sorted, sub-angular, quartz rich, planar cross-bedding with dip angles = 10°NE, 9°NE, 13°NE, 8°E, 13°E, 6°E and 21°E
Rock Pillar #5 ("Muen Sing Khon"), UTM Grid 47Q 817390/1778244, Date: 29 March 2011		
560–900 (top) (340)	MHK-076, MHK-075	Brownish white, medium grained sandstone with granules (rare), well sorted sub-round to sub-angular, quartz rich, magnetite rare, sand nodules in the lower part, trough cross-bedding cross-bedding dip angles 8°NE, 7°NE, 9°NE, 15°E and 16°E, sharp contact at the bottom surface
400–560 (160)	MHK-077	Brown white, medium-coarse grained sandstone with granules, moderately sorted, sub-angular to angular, quartz rich, magnetite, sand nodules, planar cross-bedding, erosional bottom surface contact, a lot of holes at the surface of the lower part
240–400 (160)	MHK-078	Brown white, medium grained sandstone with granules, moderately sorted, sub-angular to sub-rounded, quartz rich (pink), magnetite rare, large scale planar cross-bedding, sharp contact bottom surface
125–240 (115)	–	Brownish white, coarse grained sandstone with granules, moderately sorted, sub-angular, quartz rich, magnetite rare (prismatic habit), Fe-oxide stained sand nodules (brown), sharp bottom surface contact, a lot of holes (trace of mud and sand nodules), trough cross-bedding, bedding plane = strike N50W dip 20°E
(bottom) 0–125/(125)	–	Brownish white, medium-coarse grained sandstone with granules, moderately sorted, sub-angular, quartz rich, magnetite rare, large scale planar cross-bedding, holes at the surface

3.4. Geochemical data

3.4.1. Major elements

In Table 5, SiO_2 values range from 62.37 to 97.24 wt%. The maximum value in sample MHK-074. TiO_2 ranges from 0.06 to 0.76 wt%. Al_2O_3 ranges from 2.06 to 17.45 wt%. $Fe_2O_{3(Total)}$ from 0.08 to 7.14 wt% whereas MnO, MgO and CaO are low. Na_2O, K_2O and P_2O_5 range from 0.02 to 4.01 wt%, 0.04 to 3.45 wt% and 0.01 to 2.31 wt%, respectively. The large variation in major element contents for all of MHK samples typifies weathered rocks. Chemistry correlates strongly with grain size, because most elements display marked linear trends on the Al_2O_3 variation diagram (see Harker variation diagrams Fig. 6). In general, most elements increase as Al_2O_3 increases from sandstone to argillites. The TiO_2, Al_2O_3,

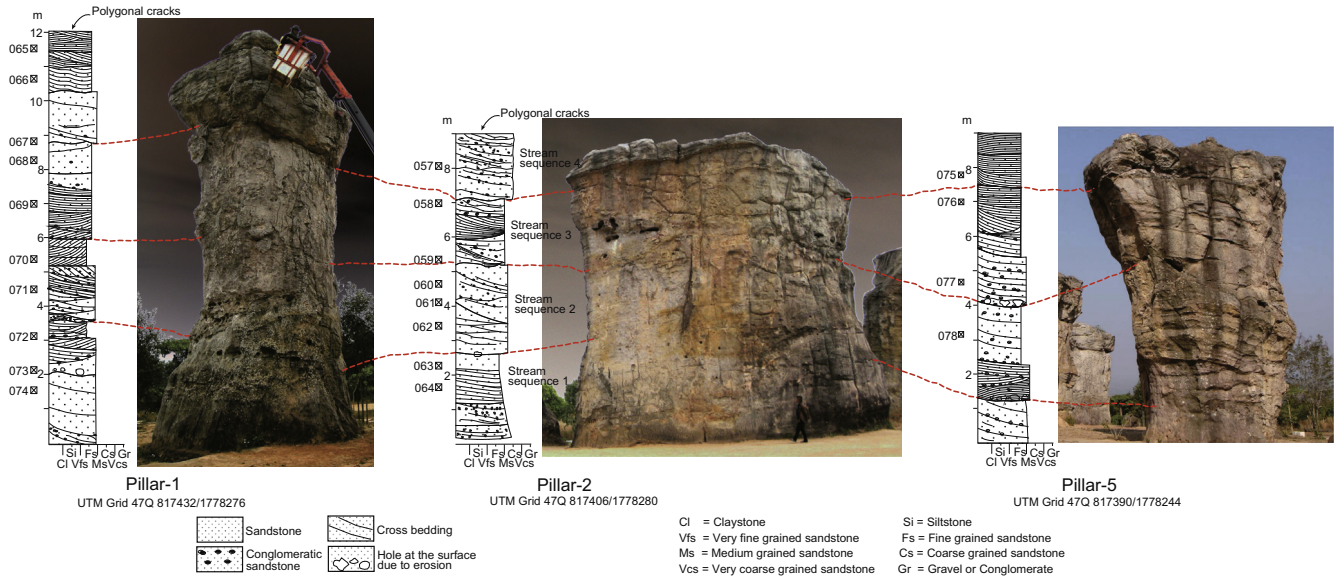

Fig. 2. The stratigraphic columns of 3 out of 5 pillars, #1 (“Khun Sri Wichai”), #2 (“Pu Rue Si”) and #5 (Muen Sing Khon) at Mo Hin Khao, showing medium-coarse grained sandstone disseminated with granules, cross-bedding, fining upwards graded bedding of 4 different sequences. The perimeter at the base of the largest pillar is 27.67 m and the tallest one is 12 m. (*Note:* three digit numbers and square symbols on the left of each figure represent the sample number.)

Fe_2O_3, MgO, CaO, Na_2O, and K_2O decrease with increase of SiO_2 content, suggesting that samples increase in their mineralogical maturity or quartzose contents but decrease in immature detrital grains (e.g. feldspar and rock fragments). Cratonic and recycled sediments associated with passive margins are higher in silica (>85% SiO_2 and 65–95% SiO_2 respectively), whereas arc-derived sediments within active orogenic margins normally contain relatively lower silica (47–82% SiO_2). Arc-derived sediments are also higher in Fe, Mg, Ti, and Al than in cratonic and recycled sediments (Bhatia, 1983). Our samples fall in the range of recycled sediments. The log (Fe_2O_3/K_2O) against Log (SiO_2/Al_2O_3) plots (Herron, 1988) fall mainly in the litharenite and sublitharenite fields with some in the subarkose and arkose fields (Fig. 7).

3.4.2. Weathering in the source area

The CIA index values of the studied samples after Nesbitt and Young (1982) vary considerably from 47 to 98, indicating significant variations in the degree of chemical weathering (Table 5). Two samples (MHK-016 and MHK-018) have high CaO values of 1.13 wt% and 1.89 wt%, respectively, which yielded low CIA values (47% and 50%, respectively). Most studied samples show moderate to high CIA (Fig. 8).

3.4.3. Trace elements

Eleven trace element concentrations (Table 5) show Ba, Sr, Cr and Zr contents are prominent with average values of 451, 149, 120 and 120 ppm respectively, while Ni, V, Rb, Y, Nb, Th and Sc have average values of 32, 33, 25, 17, 33, 6 and 4 ppm, respectively. These concentrations are below those in average Upper Continental Crust (UCC), with the exception of Si, Nb, Cr and Ni contents (Fig. 9). Contents of Na and Mg and large ion lithophile, LIL (K, Rb and Ba) elements are depleted in the samples. The High field-strength elements (HFSE), Th, Nb, Zr and Y, lack consistent interrelationships but most are slightly depleted. Nb and SiO_2 contents show positive correlation, but negative correlation to most major elements (e.g. Fe_2O_3, K_2O and MgO). However, the ferromagnesian trace elements (V, Ti, Sc, Cr and Ni) show positive correlation to each other (Table 6). These relationships demonstrate the chemical coherence and uniformity of the sediments.

4. Interpretation

4.1. Provenance

4.1.1. Heavy mineral detrital grains vs. possible sources

Six amphibole analyses plotted in the classification diagram of $Mg/(Mg + Fe^{2+})$ against Si (Leake et al., 1997), not shown here, fall in three different fields (cummingtonite, ferrogedrite and gedrite), suggesting potential derivation from different lithologies. Tourmaline and zircon provide greater constraints on the nature of the source lithologies (Morton and Hallsworth, 1994). The tourmaline group is “ultrastable” with dravite and uvite typically metamorphic or metasomatic in origin, and schorl and elbaite having granitic or pegmatitic parageneses (Morton, 1991). This mineral is stable in both weathering and diagenetic environments (Morton and Hallsworth, 1999, 2007). Its geochemistry can be applied to provenance analysis of any sandstone, irrespective of modifications during the sedimentary cycle. The different compositions make tourmaline mineral ideal for geochemical discrimination of provenance (Mange and Morton, 2007). Two analyses of tourmaline of sample MHK-059 plotted on a Al–$Fe_{(tot)}$–Mg diagram (Henry and Guidotti, 1985), not shown here, fall in the field of Li-poor granitoids and their associated pegmatites and aplites.

Owen (1987) proposed that Hf contents in detrital zircons could be used to discriminate provenance. Ahrens and Erlank (1969) gave a range in HfO_2 values from ~0.7 to 8.3 wt%, with an average of 2.0 wt%. Later, Wang et al. (2010) found that HfO_2 contents of granitic zircon (2201 analyses) range from 0.55 to 9.91 wt% with an average of 1.60 wt%. The Zr/Hf ratio in granitic zircon ranges from 4.9 to 104, with an average of 39.4. In the present study, six grains/analyses in sample MHK-020, HfO_2 ranged from 1.07 to 1.68 wt% (average 1.31 wt%) and Zr/Hf ranged from 64 to 101 (average of 84) which fall in the range of granitic zircon.

4.1.2. Possible source rock compositions regarding the rock geochemistry

In the studied samples, TiO_2 contents increase with Al_2O_3 ($r = 0.8$), suggesting an association with phyllosilicates, such as illite (Dabard, 1990). If the Al_2O_3 resides in feldspars and TiO_2 in mafic minerals, the Al_2O_3/TiO_2 range of 13–104 (average 36) indicates

Table 2
Lithological description for the rocks of the escarpment and a part of dipslope at Mo Hin Khao area.

Depth (thickness) in cm	Sample	Description
Section-01, (at "Pha Hua Nag"), 0–1430 cm at UTM Grid 47Q 815372/1777090; 1430–2330 cm at UTM Grid 47Q 815373/1777058, Date: 27 February 2011		
1770–2330 (top) (560)	MHK-11-15	Grayish white, medium to coarse grained sandstone, interbedded of thin and hard coarse grained sandstone (MHK-13) and thin fine grained sandstone (MHK-14), quartz rich, moderately weathered, horizontal bed, fining upward, bedding plane N10W dip 6–9°E
1430–1770 (340)	MHK-10	Grayish white, coarse to very coarse grained sandstone, quartz rich, moderately weathered, horizontal bed, fining upward
620–1430 (810)	MHK-09	*Upper part:* Grayish white, very coarse grained sandstone with granules, moderately weathered *Lower part:* Grayish white, conglomerate, erosional bottom, Fe-oxide cement (secondary cement and bulb or mold), erosional bottom, planar cross-bedding
570–620 (50)	MHK-08	White, homogeneous clay, high weathered, recent plant roots, and worm burrows, homogeneous
370–570 (200)	MHK-07	whitish gray, medium to coarse grained sandstone, quartz, mica, horizontal bed
330–370 (40)	MHK-06	Whitish gray, conglomerate (lens, 10 m long), mud nodules, moderately weathered, erosional bottom, sole marks
170–330 (160)	MHK-04, MHK-05	*Upper part:* Brownish gray, medium to coarse grained sandstone, quartz, magnetite, mica (slightly), lamination on upper part, erosional bottom surface *Lower part:* Basal conglomerate (50 cm thick), erosional bottom, Fe-oxide stain
100–170 (70)	MHK-02, MHK-03	Green, fine grained and homogeneous sandstone, higher resistant bed and interbedded with thin layer of mudstone, Fe-oxide stain in fractures, fining upward, bedding plane N50E dip 4°SE
(bottom) 0–100 (100)	MHK-01	Yellowish green, siltstone, moisture, mica flakes, weathered surface with Fe- and Mn-oxide stain, fissility structure
Section-02, (Escarpment pathway 1), UTM Grid 47Q 815774/1778002, Date: 28 February 2011		
1250–1775 (top) (525)	MHK-22	Reddish purple, siltstone, highly weathered, quartz rich, mica rich (muscovite), Mn-oxide filled in cross-bedding, tiny yellow spot, ripple, trough cross lamination through out of the bed, friable
650–1250 (600)	–	Gray, medium grained sandstone, alteration product of Fe-oxide (abundant), magnetite, mica rare and quartz rich, large scale of planar cross-bedding
410–650 (240)	MHK-20, MHK-21	Gray, medium grained sandstone, alteration product of Fe-oxide (abundant), magnetite, mica rare, quartz rich, medium scale of planar cross-bedding, exfoliation fracture
210–410 (200)	MHK-19	Gray, medium grained sandstone, alteration product of Fe-oxide (tiny spot of yellowish brown), magnetite, mica and quartz rich, cross-bedding plane = N2E dip 11°NW, cross-bedding dip = 20°N, 17°N, 14°N, 11°N, 8°N, 8°N, 12°N, 11°N, 11°N, 10°N, 13°N, 15°N, 16°N, and 3°N, small scale of planar cross-bedding (1–3 cm/set), bedding plane N20E dip 10–20°E, N35E dip 8°E and N22E dip 7°E
100–210 (110)	MHK-18	Whitish gray, fine grained sandstone, alteration product of ore (Fe?), magnetite, mica, quartz rich, moderately weathered, normally horizontal bed and slightly low angle of planar cross-bedding (upper part)
50–100 (50)	MHK-17	Brownish gray, very fine grained sandstone, mica rich, quartz rich, magnetite, Fe- and Mn-oxides, moderately weathered, horizontal lamination, fissility fracture
(bottom) 0–50 (50)	MHK-16	Brownish gray, siltstone to very fine grained sandstone, magnetite, Fe- and Mn-oxides, mica and quartz rich, moderately weathered, ripple and trough cross lamination
Section-03		
UTM Grid 47Q 815810/1778463, Date: 27 March 2011 ("Larn Hin Larnpee" on the dipslope)		
20,500–21,000 (top) (500)	MHK-56	White, very coarse grained sandstone with granules, quartz rich, mica rare, magnetite rare, Fe-oxide, clay and sand nodules, sub-round, cross-bedding dip angle = 12°E, 20°E, 18°E, 6°E, 15°E, tabular and large scale planar cross-bedding, bedding plane = N60E dip 11°E
UTM Grid 47Q 815787/1778454, Date: 27 March 2011 (Escarpment 5)		
19,900–20,500 (600)	MHK-54, MHK-55	White, medium grained sandstone, quartz rich, mica rare, magnetite rare, Fe-oxide, clay nodules in lower part and hole or socket of nodules, horizontal bedding, planar cross-bedding in lower part, fining upward
19,625–19,900 (275)	MHK-52, MHK-53	White, medium grained sandstone, quartz rich, mica rare, magnetite rare, Fe-oxide, lamination, bedding plane = N30E dip 9°E
UTM Grid 47Q 815749/1778614, Date: 27 March 2011 (Escarpment 4)		
17,225–19,625 (top) (2400)	–	No data
16,625–17,225 (600)	MHK-51	White (oxidized surface = brown), medium grained sandstone, quartz, green mineral, mica very rare, trace of plant fossils (carbon film), cross-bedding plane = NS dip 12°E, cross-bedding dip angles = 8°N, 12°S, 11°N, 8°N, 5°N, 8°N, large scale planar cross-bedding in upper part, tabular and large scale planar cross-bedding, erosional bottom, bedding plane = N30E dip 29°E and N11E dip 14°E
16,500–16,625 (125)	MHK-50	White (oxidized surface = brown), medium-coarse grained sandstone, clay clast in upper part, petrified wood fragments (with Fe-oxide), quartz, large scale of planar cross-bedding, set = 1 m, co-set = 2–10 cm
UTM Grid 47Q 815732/1778555, Date: 27 March 2011 (Escarpment 3)		
15,135–16,500 (1365)	–	No data
14,935–15,135 (200)	MHK-49	White (oxidized surface = brown), fine-medium grained sandstone, clay clast in lower part, tiny spot from alteration product of Fe-oxide (yellowish brown), quartz, magnetite, mica rich (in boundary of bed), low angle and large scale planar cross-bedding
14,535–14,935 (400)	MHK-48	White (oxidized surface = brown), fine-medium grained sandstone, tiny spot from alteration product of Fe-oxide (yellowish brown), quartz, magnetite, mica rich (in boundary of bed), trough cross-bedding in lower part, lamination
UTM Grid 47Q 815713/1778631, Date: 02 March 2011 (Escarpment 2)		
14,375–14,535 (160)	–	White (oxidized surface = brown), fine-medium grained sandstone, quartz, magnetite, mica rich (in boundary of bed), horizontal bed

Table 2 (*continued*)

Depth (thickness) in cm	Sample	Description
14,175–14,375 (200)	MHK-47	White (oxidized surface = brown), medium grained sandstone, clay clast, quartz, magnetite, trough cross-bedding
14,050–14,175 (125)	MHK-46	White (oxidized surface = brown), coarse grained sandstone, tiny spots of Fe-oxide (yellowish brown), quartz, magnetite, sole marks, trough cross-bedding, erosional bottom
13,885–14,050 (165)	–	White (oxidized surface = brown), medium-coarse grained sandstone, quartz, magnetite, medium scale of planar cross-bedding, co-set = 3–8 cm
13,725–13,885 (160)	MHK-45	White (oxidized surface = brown), fine grained sandstone, quartz, magnetite, medium scale of trough cross-bedding, set = 20–40 cm, co-set = 1–3 cm, direction N–S
13,630–13,725 (95)	–	White (oxidized surface = brown), medium-coarse grained sandstone, tiny spot from alteration product of Fe-oxide (yellowish brown), quartz, magnetite, large scale of trough cross-bedding, erosional bottom
13,450–13,630 (180)	MHK-44	White (oxidized surface = brown), fine-medium grained sandstone, tiny spots of Fe-oxide (yellowish brown), quartz, magnetite, mica rare, trough cross-bedding, set = 20 cm and co-set = 1 mm
13,035–13,450 (415)	MHK-43	White (oxidized surface = brown), medium-coarse grained sandstone, tiny spots of Fe-oxide (yellowish brown), quartz, magnetite, large scale of planar cross-bedding, direction N in lower part and S in upper part
12,970–13,035 (65)	–	Brown, medium grained sandstone with mud clast (1 mm diameter) in upper part, tiny spots Fe-oxide (yellowish brown), quartz, magnetite, lamination (2 mm)
12,930–12,970 (40)	MHK-42	White, coarse grained sandstone with mud clast (0.2 mm–1 cm diameter), Fe-oxide (brown), quartz, magnetite, planar cross-bedding, erosional bottom
12,770–12,930 (160)	MHK-41	White, fine-medium grained sandstone, tiny spots from alteration product of Fe-oxide (yellowish brown), quartz, magnetite, low angle planar cross-bedding
11,970–12,770 (800)	–	No data
11,850–11,970 (120)	–	Greenish yellow, fine-medium grained sandstone, tiny spots of Fe-oxide (yellowish brown), quartz, mica rich (flakes) deposited between bed contact, black (magnetite) and green mineral, large scale of planar cross-bedding, set = 40 cm and co-set = 0.5–3 cm, dip N
11,650–11,850 (200)	MHK-40	Greenish gray, fine-medium grained sandstone, tiny spot from alteration product of Fe-oxide (yellowish brown), quartz, mica rich (flakes), medium scale of planar cross-bedding (24° angle), set = 25 cm and co-set = 0.5–2 cm
11,600–11,650 (50)	–	Yellow, tiny spots of Fe-oxide, quartz, lamination (2 mm thick)
11,435–11,600 (165)	–	Yellow, fine-medium grained sandstone, Fe-oxide, quartz, mica rare, magnetite, horizontal bedding, low angle planar cross-bedding, co-set = 0.2–0.5 cm in lower part, horizontal bedding, low angle planar cross-bedding, co-set = 0.2–0.5 cm in lower part
11,310–11,435 (125)	MHK-39	Greenish brown, medium grained sandstone with mud clasts in upper part (0.2 mm–1 cm diameter), Fe-oxide, quartz, mica rare, magnetite, plant debris and coal, low angle planar cross-bedding, set = 2–5 cm and co-set = 0.5 cm
10,980–11,310 (330)	MHK-38	Greenish brown, fine grained sandstone with mud clasts in upper part (0.2 mm–1 cm diameter), Fe-oxide, quartz, mica, magnetite, low angle planar cross-bedding, co-set = 2 cm
UTM Grid 47Q 815560/1778692), Date: 01 March 2011 (Escarpment 1)		
10,945–10,980 (35)	MHK-37	Greenish brown, Fe-oxide, trough cross lamination
10,805–10,945 (140)	MHK-36	Grayish yellow, medium grained sandstone, quartz, mica rare, magnetite, planar cross-bedding in lower and horizontal lamination in upper part
10,725–10,805 (80)	–	Greenish brown, very fine grained sandstone, quartz, feldspar, mica, lamination
10,690–10,725 (35)	MHK-35	Grayish brown, mudstone, plant debris, quartz, mica, ripple, spheroidal fracture
10,550–10,690 (140)	–	Greenish brown, very fine grained sandstone, quartz, feldspar, mica, lamination
10,520–10,550 (30)	MHK-34	Grayish brown, mudstone, plant debris, quartz, mica, ripple, spheroidal fracture
9950–10,520 (570)	–	Greenish brown, very fine grained sandstone, quartz, feldspar, mica, magnetite, lamination
9030–9950 (920)	–	Yellowish brown, medium grained sandstone, quartz rich, magnetite, planar cross-bedding direction; dip N
8930–9030 (100)	–	Yellowish brown, medium grained sandstone, quartz rich, magnetite, cross-bedding direction; dip N, low angle planar cross-bedding, fining upward
8800–8930 (130)	–	Yellowish brown, fine grained sandstone, quartz rich, magnetite, horizontal bedding
8505–8800 (295)	–	Yellowish brown, medium grained sandstone, quartz rich, magnetite, tabular cross-bedding (dip N)
8455–8505 (50)	MHK-33	Yellowish brown, fine grained sandstone, quartz rich, magnetite, lamination, bedding plane N12E dip 6°SE
7340–8455 (1115)	MHK-32	Yellowish brown, medium grained sandstone, mud nodules that found only the sampling bed (50 cm thick), quartz rich, magnetite, cross-bedding direction; dip = 15°N, 5°N, 9°S, 1°S, medium-large scale of trough cross-bedding, bedding plane = N14E dip 18°SE
7270–7340 (70)	MHK-31	Yellowish brown, very coarse grained sandstone with slightly granules, mud nodules, quartz rich, planar cross-bedding, erosional bottom
6900–7270 (370)	–	Reddish purple claystone, spheroidal fracture
6750–6900 (150)	MHK-30	Reddish purple, siltstone, quartz rich and mica rich, highly weathered, trough cross lamination, spheroidal fracture
6430–6750 (320)	–	Reddish purple, claystone–siltstone, very thin beds with green claystone lens, spheroidal fracture
6290–6430 (140)	–	Reddish purple, siltstone and very fine grained sandstone (lens is about 20–35 cm in thick), quartz rich, mica rare, sandstone lens show lamination and spheroidal fracture, sand lens, spheroidal fracture, bedding plane N30E dip 12°SE
6110–6290 (180)	MHK-29	Reddish purple, siltstone, quartz rich, mica, Fe-oxide, ripple, spheroidal fracture
6080–6110 (30)	–	Reddish purple, siltstone, quartz rich, tiny mica, Fe-oxide, lamination, fissility fracture
6060–6080 (20)	–	Reddish purple, claystone
6000–6060 (60)	MHK-28	Reddish purple, very fine grained sandstone, quartz rich, tiny mica, Fe-oxide, trough cross lamination on upper part, massive
5400–6000 (600)	MHK-27	Greenish gray, claystone, highly weathered, quartz rich, mica, ripple

(*continued on next page*)

Table 2 (*continued*)

Depth (thickness) in cm	Sample	Description
4700–5400 (700)	MHK-25, MHK-26	Reddish purple, claystone–siltstone, highly weathered, quartz rich, mica rich, spheroidal fracture, fining upward
(bottom) 0–4700 (4700)	MHK-23, MHK-24	Reddish purple, siltstone, highly weathered, quartz rich, mica rich (foliation of mica flakes) (muscovite), Mn-oxide, ripple, spheroidal fracture

Fig. 3. (a) and (b) Escarpment of Mo Hin Khao, (a) tabular cross-bedding in sandstone, (b) spheroidal shattering by physical weathering of siltstone near the bottom of the escarpment. (c), (d) and (e), at Ban Non Toom, Nong Bua Daeng district, (c) dinosaur foot prints on the bedding surface, (d) close-up of the upper bed overlying the bed in (c), calcareous maroon to brown siltstone with plant roots and bivalve fossils, (e) close-up of the bed in (d), maroon, very fine to fine grained sandstones, calcareous, footprints and bones, ripple marks in the lower part.

likely felsic sources (Mishra and Sen, 2012). This interpretation is supported by the low values of MgO in the Mo Hin Khao area. The samples show a higher K_2O/Na_2O ratio (0.4–31, average 6) (Table 5 and Fig. 10), indicating quartz rich sediments. However, some concentration of $Fe_2O_{3(Total)}$ (0.08–7.14, average 1.86 wt%) in the samples could reflect presence of ferruginous cement.

K_2O/Al_2O_3 ratios can indicate relative abundance of alkali feldspar over plagioclase and clay minerals. Ratios >0.5 suggest a significant quantity of alkali feldspar relative to other aluminosilicates. In contrast, K_2O/Al_2O_3 ratios <0.4 suggest a lack of alkali feldspar in the rocks (Cox et al., 1995). The studied rocks have an average K_2O/Al_2O_3 ratio of 0.1 (0.01–0.3) (Table 5). This result is consistent with low amounts of feldspar. The high proportion of quartz and the dominance of weathered K-feldspar in studied samples suggest that the source area was exposed to long-term weathering and that the sediments were at least partly polycyclic.

To infer provenance, discriminant function scores of the samples (F1 and F2) for major elements were plotted within the fields proposed by Roser and Korsch (1988) (Fig. 11). The analyzed samples lie mainly in the field of quartzose sedimentary provenance;

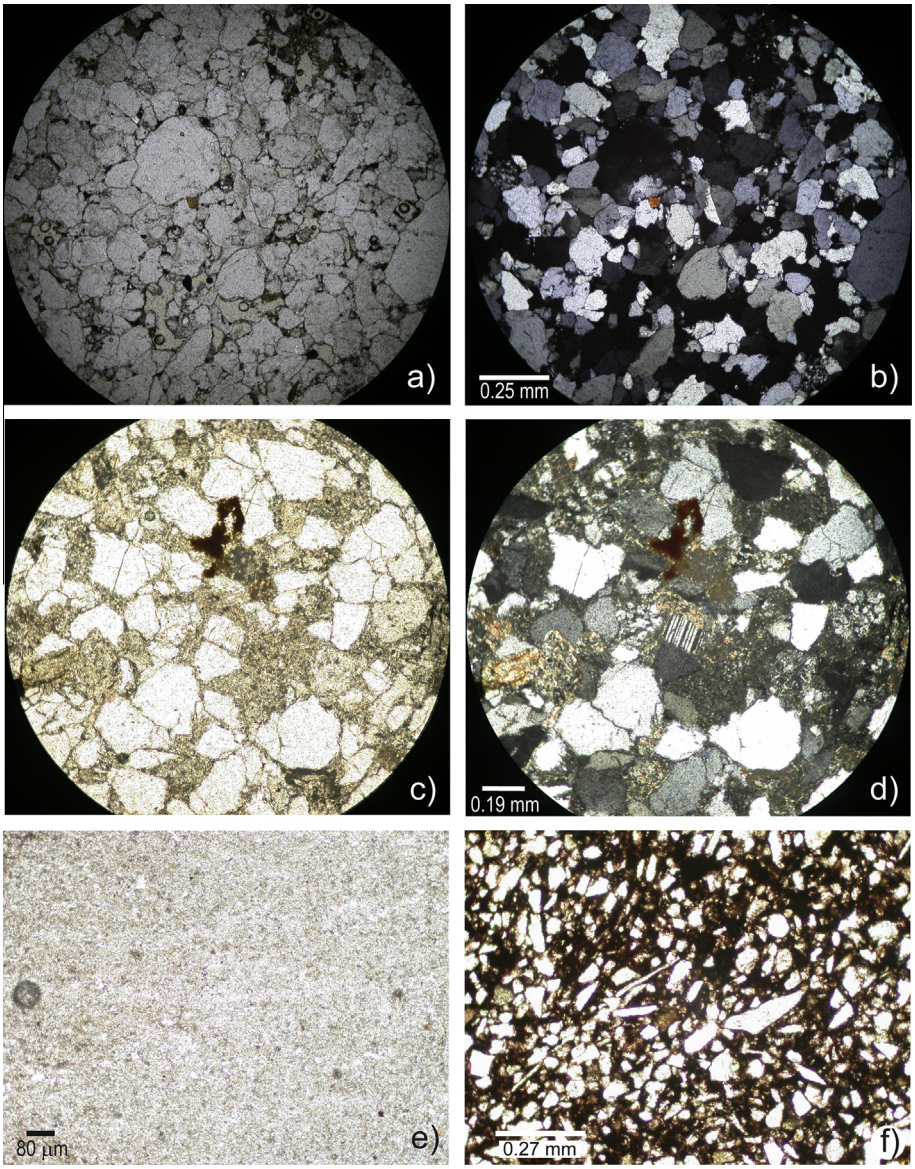

Fig. 4. Photomicrographs, (a) sample MHK-058, PPL (plane polarization) image showing sub-round to sub-angular quartz grains. The lithic grains of chert composing of microquartz found in the middle left and lower left of the image. A tiny greenish brown grain of amphibole appears in the middle, (b) XPL (cross polarization) image of sample MHK-058; (c) sample MHK-020, PPL, showing the quartz grains with sub-angular outline, very well sorted, the cementing materials (clay minerals, 2nd mica and Fe-oxides) are higher percentage than those of the upper beds on the dipslope, (d) XPL of sample MHK-020, plagioclase crystal showing polysynthetic twin in the middle of the image; (e) PPL of sample BNT-001, mudstone showing very fine grains containing the calcareous clay, (f) PPL of sample BNT-002, fine grained calcareous sandstone showing a texture indicating the water current and clear angular to sub-rounded quartz grains with reddish brown of Fe-oxide cementing material and the two mica grains seen as the long thin needle-like crystals along the diagonal of the image. (For interpretation of the references to color in this figure legend, the reader is referred to the web version of this article.)

except for two samples falling separately in intermediate igneous and felsic igneous provenances. The recycled nature of the studied sediments is also reflected in the sandstone modal compositions (Fig. 5), being dominantly litharenite and sublitharenite composition with abundant sedimentary lithics, lacking feldspar and heavy minerals. Fig. 11 indicates that the studied sediments were reworked or recycled from older sediments (Diskin et al., 2011), perhaps, from a quartzose sedimentary provenance (Roser and Korsch, 1988). This field represents recycled-mature polycyclic quartzose detritus and the recycled sources represent quartzose sediments of mature continental provenance. The sediments could be derived from a highly weathered granite terrain and/or from a pre-existing sedimentary terrain (Roser and Korsch, 1988; Rahman and Suzuki, 2007), as in the Greenland Group of New Zealand (Roser and Korsch, 1988). The closest parent material before deposition in the area would probably have been the higher quartz content sedimentary rocks e.g. older sandstones, probably the Triassic or Jurassic detrital sedimentary rocks in the Khorat Group. A high percentage of quartzose sediment suggests a continental source (Roser and Korsch, 1986, 1988; Tucker, 2001; Rahman and Suzuki, 2007; Yan et al., 2007; Concepcion et al., 2012).

The geochemistry of the siliciclastic sediments of the present study suggests the effect of severe weathering with sediment recycling. The ferromagnesian trace elements Cr, Ni and V are generally compatible in magmatic processes, but can be fractionated during weathering (Feng and Kerrich, 1990). Weber and Middleton (1961a,b) suggested that Ni is principally derived from easily disintegrated pyroxene, olivine and serpentine (Garver et al., 1996). In the studied samples, Cr and Ni exceed the average composition of UCC. This enrichment may suggest some basic rock input from the source terrain. Generally values of Cr (>150 ppm) and Ni (>100 ppm), ratio of Cr/Ni between 1.3 and 1.5 and a high

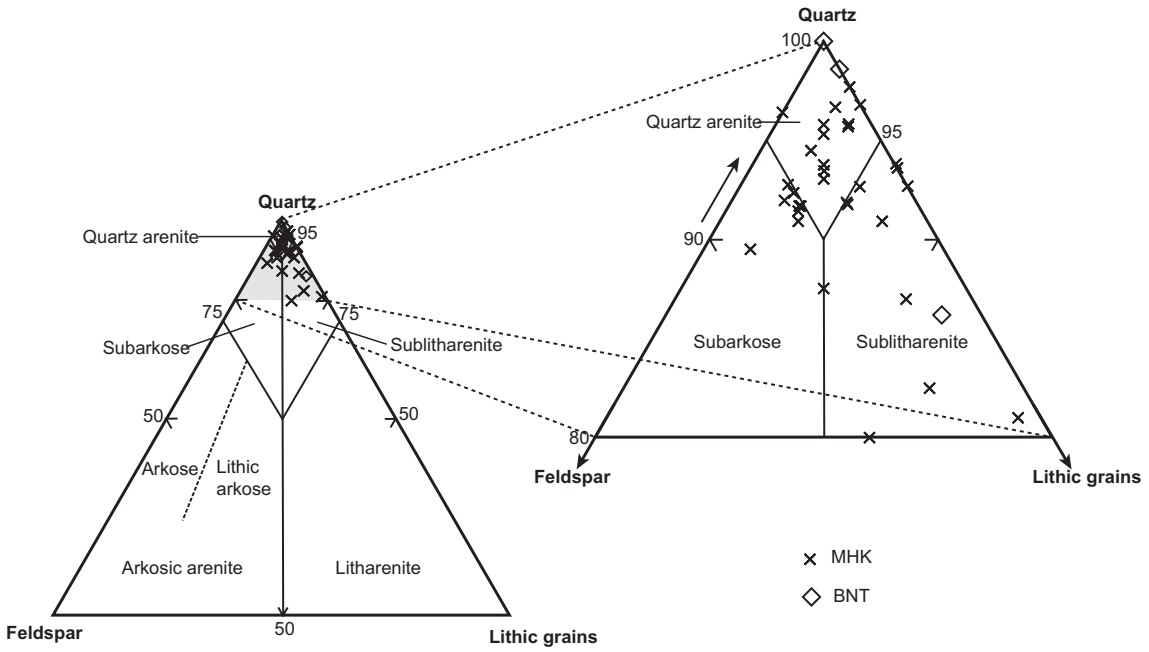

Fig. 5. Q–F–L diagram of the studied samples. Fields in diagram are from Pettijohn et al. (1987), (MHK = Mo Hin Khao; BNT = Ban Non Toom).

Table 3
List of minerals in the samples identified by the XRD.

Sample ID	Quartz	Albite	Calcite	Dolomite	Kaolinite	Chlorite	Mica[a]
BNT-001	√	–	√	√	–	√	√
BNT-002	√	√	√	–	–	–	√
BNT-003	√	√	√	–	–	–	√
MHK-001	√	–	–	–	–	√	√
MHK-008	√	–	–	–	√	–	√
MHK-016	√	√	–	–	√	–	√
MHK-026	√	√	–	–	–	–	√
MHK-027	√	√	–	–	–	–	√
MHK-029	√	√	–	–	–	–	√
MHK-031	√	√	–	–	–	–	√
MHK-034	√	√	–	–	–	–	√
MHK-039	√	√	–	–	–	–	√
MHK-042	√	√	–	–	√	–	√
MHK-022	√	√	–	–	√	–	√

[a] Mica is for muscovite and illite.

correlation coefficient between Cr and Ni in shales, are diagnostic of ultramafic rocks in the source area, whereas higher Cr/Ni ratios (~2 or higher) indicate mafic volcanic detritus. Cr/Ni ratios of >3 for sandstones suggest significant sedimentary fractionation (Garver et al., 1996). In this study, Cr ranges from 74 to 160 ppm (average 120 ppm), Ni ranges from 18 to 71 ppm (average 32 ppm) and Cr/Ni ratios vary from 2 to 7 (average 4) (Table 5). Thus the existence of widespread mafic/ultramafic rocks in the source region was most unlikely (cf. Rahman and Suzuki, 2007). The observed values are more likely to be fractionated during weathering. The absence of detrital chrome spinel within the studied rock samples, as revealed from heavy mineral data is consistent with this finding. Accessory magnetite detrital grains in our samples and may come from basic volcanic rocks.

High field strength elements (HFSE), e.g. Y, Sc, Th, Zr, Hf, Ti, Nb are well suited for provenance and tectonic setting determinations because of their relatively low mobility during sedimentary processes (weathering, transport, diagenesis) and metamorphism, and their low residence time in sea water/water columns (Holland, 1978). They are transported quantitatively into clastic sedimentary rocks during weathering and transportation and provide a signature of the parent material (McLennan et al., 1983); thus they are transferred (almost) quantitatively into the sedimentary record. Ratios of both incompatible and compatible elements are useful for differentiating between felsic and mafic source components (Nyakairu and Koeberl, 2001).

The HFSE are preferentially partitioned into melts during crystallization (Feng and Kerrich, 1990) and then enriched in felsic rather than mafic sources. These elements are thought to reflect provenance compositions through their generally immobile behavior (Taylor and McLennan, 1985). Th abundance is higher in felsic than in mafic igneous source rocks and in their weathered products, whereas Sc and Cr are more concentrated in mafic than in felsic igneous rocks and in their weathered products (Taylor and McLennan, 1985; Wronkiewicz and Condie, 1987). The relative enrichments of incompatible elements, e.g. Th over compatible elements, e.g. Sc in the sediments, indicate relatively felsic average provenance compositions and a relatively severe weathering regime (McLennan et al., 1993). Mafic and felsic source rocks may lead to significantly different ratios of, for example Th/Sc and Cr/Th, and hence, provide useful information about the provenance of sedimentary rocks (e.g., Cullers et al., 1988; Cullers, 1994,

Table 4
Electron probe microanalyses (EPMA) of minerals in sandstones of Mo Hin Khao (oxides in wt%).

Mineral/grain type	Quart, detrital grain	Micro quartz in chert (lithic fragment)	Albite	Orthocalse
Analysis no.	4	6	23	30
Sample ID	MHK-059_QTZ1_01	MHK-059_MQTZ1_01	MHK-020_Plag1_01	MHK-031_Feld1_01
SiO_2	98.73	99.68	67.72	64.58
TiO_2	0.033	0.012	0.02	1.33
Al_2O_3	0	0.15	17.86	19.43
Fe_2O_3[a]	0.01	0	0.06	1.47
MnO	0.01	0	0	0.02
MgO	0	0	0	0.75
CaO	0	0	0.26	0.05
Na_2O	0	0	12.16	0
K_2O	0	0.01	0.05	11.97
P_2O_5	0.03	0.01	0	0.01
NiO	0.04	0	0.06	0.01
Cr_2O_3	0	0.02	0.04	0
Cl	0	0.03	0.02	0.15
ZnO	0	0.04	0.07	0
Total	98.86	99.94	98.31	99.78
Numbers of ions on the basis of 32 O				
Si	15.986	15.968	12.081	11.723
Ti	0.004	0.001	0.002	0.181
Al	0	0.027	3.754	4.157
Fe^{3+}	0.002	0	0.008	0.201
Mn	0.002	0	0.001	0.002
Mg	0	0	0	0.204
Ca	0.001	0	0.05	0.011
Na	0	0	4.206	0
K	0.001	0.001	0.01	2.772
P	0.004	0.001	0	0.002
Ni	0.005	0	0.008	0.001
Cr	0	0.002	0.005	0
Cl	0	0.009	0.006	0.046
Zn	0	0.004	0.009	0.001
Total	16.004	16.015	20.141	19.3
End members				
An	–	–	1.2	0.4
Ab	–	–	98.6	0
Or	–	–	0.2	99.6

Mineral/grain type	Muscovite	Mineral/grain type	Tourmaline	Mineral/grain type	Zircon
Analysis no.	12	Analysis no.	9	Analysis no.	16
Sample ID	MHK-059_Mica1_01	Sample ID	MHK-059_Tour1_01	Sample ID	MHK-020_Zir3_01
SiO_2	48.67	SiO_2	35.96	SiO_2	35.65
TiO_2	0.19	TiO_2	0.69	ZrO_2	62.04
Al_2O_3	33.59	B_2O_3	10.25	HfO_2	1.31
FeO	2.94	Al_2O_3	31.82	TiO_2	0.24
MnO	0.04	Fe_2O_3	5.03	Al_2O_3	0.01
MgO	0.8	FeO	11.71	Fe_2O_3[a]	0.20
CaO	0.05	MgO	4.07	MnO	0.01
Na_2O	0.05	CaO	0.39	K_2O	0.01
K_2O	12.36	Na_2O	0.57	Cl	0.02
P_2O_5	0.08	K_2O	0.06	ZnO	0.06
Cl	0.003	Cr_2O_3	0.02	Total	99.53
ZnO	0.02	Cl	0.01		
Total	98.8	Total	100.57		
No. of ions on the basis of 22 O, ignoring H_2O		No. of ions on the basis of 30 O		No. of ions on the basis of 16 O	
Si	7.205	Si	6.049	Si	4.281
Al	0.795	B	2.976	Zr	3.633
Al	5.065	Al	6	Hf	0.045
Ti	0.021	Al	0.309	Ti	0.021
Fe^{2+}	0.364	Fe^{3+}	0.637	Al	0.002
Mn	0.005	Mg	1.022	Fe^{3+}	0.018
Mg	0.177	Ti	0.088	Mn	0.001
Ca	0.008	Fe^{2+}	1.647	K	0.001
Na	0.014	Na	0.185	Cl	0.004
K	2.334	Ca	0.07	Zn	0.005
P	0.01	K	0.013	Total	8.011
Cl	0.001	Cr	0.003	Hf/Zr	0.01
Zn	0.002	Cl	0.003		
Total	16	Total	19		

Mineral/grain type	Magnetite	Mineral/grain type	Amphibole	Amphibole	Amphibole	Mineral/grain type	Clay mineral	Clay mineral
Analysis no.	21	Analysis no.	1	5	14	Analysis no.	8	33
Sample ID	MHK-020_Mgt2_01	Sample ID	MHK-059_AMP1_01	MHK-059_AMP2_01	MHK-020_AMP1_01	Sample ID	MHK-059_Clay1_01	MHK-031_Clay1_01
SiO_2	0.99	SiO_2	35.93	55.97	39.39	SiO_2	45.92	39.34
TiO_2	2.73	TiO_2	0.99	0	0.3	TiO_2	0.01	0.12
Al_2O_3	0.65	Al_2O_3	32.31	13.82	29.02	Al_2O_3	35.45	29.7
Fe_2O_3	63.93	Cr_2O_3	0.01	0.06	0.13	FeO	0.09	4.64
FeO	36.33	FeO	7.57	6.38	13.42	MnO	0	0.10
MnO	0	MnO	0.02	0.05	0.01	MgO	0.02	6.81
MgO	0.04	MgO	15.43	10.08	6.72	CaO	0.04	0.19
Cr_2O_3	0.07	NiO	0	0	0.09	K_2O	0.02	2.61
ZnO	0.07	ZnO	.07	0	.07	ZnO	0	0.07
Total	104.99	CaO	0.37	3.42	0.62	Cl	0	0.09
No. of ions on the basis of 32 O		Na_2O	0.5	6.01	0.71	Cr_2O_3	0.02	0
Si	0.287	K_2O	0.04	0.62	0.01	NiO	0	0.03
Ti	0.596	SrO	0	0.03	0.01	HfO_2	0	0.05
Al	0.221	Cl	0	0.09	0.01	P_2O_5	0.07	0.11
Fe^{3+}	13.967	H_2O[b]	2.10	2.15	2.00	Total	81.61	83.86
Fe^{2+}	8.821	Total	95.34	98.67	92.5	No. of ions on the basis of 22 O, ignoring H_2O		
Mn	0	O=F,Cl	0	0.02	0	Si	6.525	5.853
Mg	0.017	Total	95.34	98.65	92.5	Al	5.937	5.209
Cr	0.016	No. of ions on the basis of 23 O				Ti	0.001	0.014
Zn	0.014	Si	5.14	7.72	5.905	Fe	0.01	0.578
Total	24	Al^{iv}	2.86	0.28	2.095	Mn	0	0.012
% end-members	Al^{vi}	2.587	1.966	3.032		Mg	0.004	1.511
Spinel	0.2	Ti	0.106	0	0.034	Zn	0	0.008
Hercynite	0	Cr	0.001	0.007	0.016	Ca	0.006	0.03
Gahnite	0.2	Fe^{2+}	0.906	0.736	1.682	K	0.003	0.496
Galaxite	0	Mn	0.003	0.005	0.001	Cl	0	0.022
Magnetite	91.7	Mg	3.29	2.073	1.502	Cr	0.002	0
Chromite	0.1	Ni	0	0	0.011	Ni	0	0.003
Ulvöspinel	7.8	Zn	0.007	0	0.008	Hf	0	0.003
Total	100	Ca	0.056	0.505	0.099	P	0.008	0.014
		Na	0.139	1.608	0.205	Total	12.495	13.752
		K	0.007	0.109	0.002			
		Sr	0	0.003	0.001			
		Cl	0	0.02	0.002			
		OH[b]	2	1.98	1.998			
		Total	17.103	17.012	16.593			
		(Ca + Na) (B)	0.102	2	0.305			
		Na (B)	0.046	1.492	0.205			
		(Na + K) (A)	0.1	0.224	0.002			
		$Mg/(Mg + Fe^{2+})$	0.784	0.738	0.472			

[a] Total Fe as Fe_2O_3.
[b] From calculation (Tindle, 2012).

2000; Cullers and Podkovyrov, 2000). Ratios such as Th/Sc and Cr/Th in siliciclastic sediments can place constraints on the average provenance composition (e.g. Wronkiewicz and Condie, 1987, 1989, 1990; Cullers et al., 1988; Cullers, 1994, 1995; Cox et al., 1995). The geochemical differences between elements such as Th and La (indicative of a felsic source) and Sc and Cr (indicative of a mafic source) have been exploited to distinguish between felsic and mafic provenance (e.g. McLennan et al., 1980; McLennan, 1989; Wronkiewicz and Condie, 1990; McLennan and Taylor, 1991).

In this study the Th/Sc ratios have a wider range (0.3–157) than ratios of sediments from felsic sources although their average value (10) is still in the range. The Cr/Th values range from the higher values of sediments from felsic sources to lower values of sediments from mafic sources. This implies that the studied sediments may come from felsic to intermediate source rocks with a small component from mafic source rocks. The Th vs. Sc plot (Fig. 12) shows that most sediment data scatter above the Th/Sc = 1 line, with most samples that have Sc contents below 15 ppm, indicating a more felsic component (Nyakairu and Koeberl, 2001). The Th/Sc values of the samples exceed that of UCC (=1). The minor data group plots in between Th/Sc = 0.6 and 1 and two samples have Th/Sc < 0.6. This indicates that the sediments did not reflect a uniform provenance but a mixed source of sediments. Some sediment data plot close to the value of UCC, despite the intense weathering experienced by the sediments, indicating that Th and Sc have remained immobile. The sediments have low contents of Sc and Fe and low Th/Cr ratios but high concentrations of Cr and Th and high Th/Sc and Ba/Sc ratios. This suggests deriviation mainly from felsic rocks but does not exclude an intermediate source, or possible mixing between felsic and basic source rocks (cf. Cullers et al., 1987, 1988; Cullers, 1988). Moreover, the studied sediments show non-uniform K/Rb ratios (Fig. 13, by Shaw, 1968), in that, most samples lie close to a typical differentiated magmatic suite or main trend with a ratio of 230. This feature emphasizes the chemically coherent nature of the sediments and derivation mainly from acidic to intermediate rocks. Certain samples plot with basic source rocks and some have lower K/Rb value. This latter result may indicate derivation mainly from acidic to intermediate rocks with minor mafic input. This favors sediments derived from predominantly acidic sources. The high basic element values, e.g. Cr and Ni, probably were derived from ferromagnesian minerals such as magnetite and amphibole while the sediments predominantly suggest granitoid sources.

Th and Sc are especially useful for monitoring source area composition (Taylor and McLennan, 1985; Cullers and Podkovyrov,

Table 5
Normalised major and trace elements of Mo Hin Khao (MHK) and Ban Non Toom (BNT) clastic rocks.

Oxides (wt%)/ sample no.	BNT-001	BNT-002	BNT-003	MHK-001	MHK-002	MHK-006A	MHK-006B	MHK-011	MHK-016	MHK-018	MHK-020	MHK-022	MHK-023	MHK-026
SiO_2	62.37	81.32	79.96	69.90	87.07	88.76	91.91	97.24	80.21	92.22	87.27	90.09	89.82	76.70
TiO_2	0.50	0.42	0.46	0.76	0.56	0.35	0.35	0.12	0.43	0.10	0.35	0.28	0.29	0.61
Al_2O_3	17.45	9.32	10.49	17.17	7.48	9.83	6.13	2.36	9.18	4.03	9.72	5.73	5.32	13.17
$Fe_2O_{3(Total)}$	5.76	3.79	4.02	7.14	3.31	0.52	0.97	0.13	3.04	0.85	0.74	1.84	1.75	4.20
MnO	0.35	0.08	0.01	0.04	0.01	0.01	0.01	0.01	0.01	0.05	0.01	0.25	0.02	0.02
MgO	9.89	1.77	1.53	1.53	0.60	0.01	0.01	0.01	0.42	0.33	0.15	0.14	0.33	1.00
CaO	x	x	x	0.28	0.11	0.02	0.03	0.03	1.13	1.89	0.06	0.11	0.15	0.43
Na_2O	0.40	1.85	1.66	0.10	0.06	0.05	0.06	0.03	4.01	0.05	0.38	0.33	0.95	0.97
K_2O	3.14	0.91	1.66	2.93	0.66	0.42	0.49	0.06	1.50	0.47	1.27	1.19	1.33	2.80
P_2O_5	0.15	0.53	0.23	0.14	0.12	0.03	0.04	0.01	0.07	0.03	0.05	0.05	0.05	0.10
SUM	100.00	100.00	100.00	100.00	100.00	100.00	100.00	100.00	100.00	100.00	100.00	100.00	100.00	100.00
LOI*	29.16	10.91	7.34	5.16	3.04	3.30	2.57	0.54	4.31	4.39	2.89	2.39	2.22	3.67
Total*	100.09	99.94	100.20	100.16	100.06	100.27	99.80	100.31	100.04	100.03	100.07	99.90	99.81	100.04
SiO_2/Al_2O_3	4	9	8	4	12	9	15	41	9	23	9	16	17	6
Al_2O_3/SiO_2	0.3	0.1	0.1	0.2	0.1	0.1	0.1	0.0	0.1	0.04	0.1	0.1	0.1	0.2
$Al_2O_3/(CaO + Na_2O)$	44	5	6	46	42	127	66	39	2	2	22	13	5	9
$Fe_2O_3 + MgO$	16	6	6	9	4	1	1	0	3	1	1	2	2	5
K_2O/Na_2O	8	0.5	1	31	10	8	8	2	0.4	10	3	4	1	3
K_2O/Al_2O_3	0.2	0.1	0.2	0.2	0.1	0.0	0.1	0.02	0.2	0.1	0.1	0.2	0.3	0.2
Al_2O_3/TiO_2	35	22	23	23	13	28	17	19	21	42	28	21	18	22
CIA (%)	81	70	70	82	88	94	90	93	47	50	82	74	62	71
Trace elements (ppm)														
Ni	23	29	36	65	50	N/A	22	22	33	22	28	71	36	45
V	19	37	48	101	67	N/A	50	21	52	18	29	24	41	60
Rb	17	14	27	57	25	N/A	14	8	31	16	31	28	33	50
Y	8	19	17	22	25	N/A	17	16	22	19	16	26	23	18
Nb	22	25	26	23	32	N/A	40	40	32	35	37	28	32	27
Th	3	4	5	5	7	N/A	6	6	5	6	6	5	8	6
Cr	74	120	124	160	149	N/A	131	104	158	93	102	128	148	138
Sr	261	198	184	132	124	N/A	125	121	166	187	217	155	155	143
Ba	78	365	136	352	182	N/A	97	59	256	142	103	5963	1616	434
Sc	11	1	9	12	8	N/A	3	0.04	3	1	6	0.2	7	8
Zr	49	126	100	103	215	N/A	204	161	191	82	155	126	201	112
Th/Sc	0	3	1	0	1	N/A	2	157	2	7	1	24	1	1
Cr/Th	22	27	27	30	22	N/A	23	17	29	15	16	24	19	23
Th/Cr	0.05	0.04	0.04	0.03	0.04	N/A	0.04	0.06	0.03	0.07	0.06	0.04	0.05	0.04
Cr/Ni	3	4	3	2	3	N/A	6	5	5	4	4	2	4	3
K/Rb	1504	527	502	424	222	N/A	284	57	403	244	336	350	337	462
Rb/Sr	0.1	0.1	0.1	0.4	0.2	N/A	0.1	0.1	0.2	0.1	0.1	0.2	0.2	0.4
V/Cr	0.3	0.3	0.4	1	0.5	N/A	0.4	0.2	0.3	0.2	0.3	0.2	0.3	0.4
Ba/Sc	7	253	15	29	24	N/A	33	1482	99	151	16	27104	225	55

Oxides (wt%)/ sample no.	MHK-027	MHK-029	MHK-030	MHK-031	MHK-034	MHK-036	MHK-039	MHK-040	MHK-042	MHK-049A	MHK-049B	MHK-051A	MHK-052
SiO_2	78.19	79.05	84.43	91.63	83.22	91.15	85.36	87.61	92.24	91.65	92.52	88.73	91.36
TiO_2	0.62	0.58	0.47	0.18	0.61	0.14	0.25	0.20	0.06	0.19	0.18	0.29	0.11
Al_2O_3	11.75	11.83	7.94	5.13	9.15	5.36	9.37	7.83	5.80	5.34	4.62	8.22	7.86
$Fe_2O_{3(Total)}$	3.96	3.79	3.33	0.75	2.73	1.54	1.45	1.40	0.76	1.11	1.06	0.67	0.19
MnO	0.01	0.01	0.01	0.05	0.01	0.02	0.01	0.01	0.01	0.01	0.01	0.01	0.01
MgO	0.97	0.87	0.63	0.33	0.78	0.25	0.43	0.57	0.02	0.11	0.11	0.10	0.01
CaO	0.32	0.26	0.21	0.12	0.23	0.08	0.15	0.13	0.04	0.06	0.06	0.06	0.02
Na_2O	0.66	1.00	0.86	0.84	0.50	0.48	0.50	0.65	0.31	0.27	0.30	0.48	0.02
K_2O	3.45	2.52	2.05	0.92	2.71	0.96	2.41	1.54	0.74	1.24	1.13	1.40	0.40
P_2O_5	0.06	0.08	0.06	0.04	0.06	0.02	0.07	0.04	0.02	0.02	0.02	0.04	0.02
SUM	100.00	100.00	100.00	100.00	100.00	100.00	100.00	100.00	100.00	100.00	100.00	100.00	100.00
LOI*	3.90	3.04	2.74	1.77	3.96	4.67	2.76	2.39	1.39	1.71	1.83	2.76	3.16
Total*	99.95	99.93	99.69	99.80	100.20	99.49	100.07	100.20	99.81	99.27	100.04	99.94	99.25
SiO_2/Al_2O_3	7	7	11	18	9	17	9	11	16	17	20	11	12
Al_2O_3/SiO_2	0.2	0.1	0.1	0.1	0.1	0.1	0.1	0.1	0.1	0.1	0.0	0.1	0.1
$Al_2O_3/(CaO + Na_2O)$	12	9	7	5	12	10	14	10	17	16	13	15	184
$Fe_2O_3 + MgO$	5	5	4	1	4	2	2	2	1	1	1	1	0.2
K_2O/Na_2O	5	3	2	1	5	2	5	2	2	5	4	3	19
K_2O/Al_2O_3	0.3	0.2	0.3	0.2	0.3	0.2	0.3	0.2	0.1	0.2	0.2	0.2	0.1
Al_2O_3/TiO_2	19	20	17	28	15	37	37	38	104	27	26	28	71
CIA (%)	69	71	66	66	69	73	72	72	81	74	72	77	94
Trace elements (ppm)													
Ni	55	46	44	38	47	24	29	29	28	30	N/A	22	22
V	85	59	67	11	72	18	22	21	14	27	N/A	40	18

(*continued on next page*)

Oxides (wt%)/ sample no.	MHK-027	MHK-029	MHK-030	MHK-031	MHK-034	MHK-036	MHK-039	MHK-040	MHK-042	MHK-049A	MHK-049B	MHK-051A	MHK-052
Rb	66	47	44	22	54	22	32	32	23	28	N/A	33	16
Y	18	22	21	19	24	15	16	17	16	17	N/A	12	13
Nb	24	26	29	33	28	34	30	34	32	34	N/A	39	42
Th	6	5	7	6	7	5	5	5	5	5	N/A	3	7
Cr	145	140	133	112	158	102	107	122	99	116	N/A	112	98
Sr	141	146	153	134	137	127	128	132	128	143	N/A	203	126
Ba	314	530	1592	363	371	147	129	160	79	98	N/A	785	44
Sc	8	9	7	1	7	0.5	0.2	2	0.4	1	N/A	1	1
Zr	112	146	174	109	165	84	75	97	72	148	N/A	157	61
Th/Sc	1	1	1	4	1	11	23	3	12	5	N/A	6	10
Cr/Th	26	27	20	20	24	19	22	23	19	21	N/A	33	13
Th/Cr	0.04	0.04	0.05	0.05	0.04	0.05	0.04	0.04	0.05	0.05	N/A	0.03	0.07
Cr/Ni	3	3	3	3	3	4	4	4	4	4	N/A	5	4
K/Rb	437	446	391	354	418	364	630	404	271	364	N/A	355	207
Rb/Sr	0.5	0.3	0.3	0.2	0.4	0.2	0.2	0.2	0.2	0.2	N/A	0.2	0.1
V/Cr	0.6	0.4	1	0.1	0.5	0.2	0.2	0.2	0.1	0.2	N/A	0.4	0.2
Ba/Sc	40	62	234	265	54	300	612	95	184	81	N/A	1308	58

Oxides (wt%)/ sample no.	MHK-054	MHK-056	MHK-058	MHK-059	MHK-063	MHK-066	MHK-074	MHK-077	MHK-087	Max.	Min.	Average	NASC[a]	UCC[b]
SiO_2	92.44	94.16	94.43	93.89	95.18	93.94	96.85	94.19	95.00	97.24	62.37	87.41	64.80	66.00
TiO_2	0.09	0.06	0.09	0.08	0.08	0.13	0.09	0.08	0.10	0.76	0.06	0.29	0.70	0.50
Al_2O_3	6.83	5.53	2.06	5.61	4.32	5.05	2.48	5.05	3.11	17.45	2.06	7.56	16.90	15.20
$Fe_2O_{3(Total)}$	0.19	0.13	0.36	0.08	0.13	0.53	0.10	0.27	0.76	7.14	0.08	1.86	5.65	5.00
MnO	0.01	0.01	0.01	0.01	0.01	0.01	0.01	0.01	0.01	0.35	0.01	0.04	0.06	0.08
MgO	0.01	0.01	0.01	0.01	0.01	0.01	0.01	0.01	0.01	9.89	0.01	0.86	2.86	2.20
CaO	0.02	0.01	0.15	0.03	0.04	0.04	0.08	0.11	0.01	1.89	0.00	0.22	3.63	4.20
Na_2O	0.05	0.03	0.03	0.03	0.04	0.04	0.03	0.05	0.05	4.01	0.02	0.58	1.14	3.90
K_2O	0.35	0.04	0.54	0.09	0.09	0.16	0.10	0.14	0.04	3.45	0.04	1.19	3.97	3.40
P_2O_5	0.01	0.01	2.31	0.17	0.12	0.08	0.24	0.08	0.90	2.31	0.01	0.22	0.13	–
SUM	100.00	100.00	100.00	100.00	100.00	100.00	100.00	100.00	100.00	144.50	64.65	100.24	99.84	100.48
LOI*	0.86	0.55	1.38	0.82	0.94	0.92	1.63	1.17	1.10	29.16	0.54	4.13	–	–
Total*	100.01	99.25	100.10	99.75	99.18	100.14	99.93	100.12	100.07	100.31	99.18	99.91	99.84	100.48
SiO_2/Al_2O_3	14	17	46	17	22	19	39	19	31	46	4	16	4	4
Al_2O_3/SiO_2	0.1	0.1	0.02	0.1	0.0	0.1	0.03	0.1	0.03	0.3	0.02	0.1	0.3	0.2
$Al_2O_3/(CaO + Na_2O)$	94	137	11	90	60	64	22	32	48	184	2	39	4	2
$Fe_2O_3 + MgO$	0.2	0.1	0.4	0.1	0.1	1	0.1	0.3	1	16	0.1	3	9	7
K_2O/Na_2O	7	1	16	3	2	4	3	3	1	31	0.4	6	3	1
K_2O/Al_2O_3	0.1	0.01	0.3	0.02	0.02	0.03	0.04	0.03	0.01	0.3	0.01	0.1	0.2	0.2
Al_2O_3/TiO_2	73	88	22	69	54	40	26	62	32	104	13	36	24	30
CIA (%)	93	98	69	96	95	94	89	92	95	98	47	78	57	46
Trace elements (ppm)														
Ni	18	18	22	23	23	24	21	N/A	19	71	18	32	58	20
V	5	7	6	8	11	16	4	N/A	17	101	4	33	130	60
Rb	8	8	11	8	9	9	7	N/A	7	66	7	25	125	112
Y	10	17	12	14	16	15	13	N/A	12	26	8	17	35	22
Nb	40	40	38	39	38	40	39	N/A	39	42	22	33	13	25
Th	5	7	6	6	6	5	5	N/A	6	8	3	6	12	11
Cr	121	94	119	110	138	104	98	N/A	99	160	74	120	125	35
Sr	119	121	130	127	127	165	131	N/A	121	261	119	149	142	350
Ba	14	23	132	39	66	105	71	N/A	29	5963	14	451	636	550
Sc	3	2	1	3	0.3	1	3	N/A	2	12	0.04	4	15	11
Zr	43	90	80	80	84	129	105	N/A	112	215	43	120	200	190
Th/Sc	2	3	7	2	21	5	2	N/A	3	157	0.3	10	1	1
Cr/Th	25	14	20	19	22	19	19	N/A	17	33	13	22	10	3
Th/Cr	0.04	0.07	0.05	0.05	0.05	0.05	0.05	N/A	0.06	0.07	0.03	0.05	0.10	0.31
Cr/Ni	7	5	5	5	6	4	5	N/A	5	7	2	4	2	2
K/Rb	380	44	418	92	86	145	107	N/A	50	1504	44	352	264	252
Rb/Sr	0.1	0.1	0.1	0.1	0.1	0.1	0.1	N/A	0.1	0.5	0.1	0.2	1	0.3
V/Cr	0.0	0.1	0.05	0.1	0.1	0.2	0.04	N/A	0.2	0.6	0.04	0.3	1	2
Ba/Sc	5	11	167	12	221	93	25	N/A	14	27104	5	1010	43	50

x = the original CaO for samples BNT-001 = 29.17 wt%, BNT-002 = 10.44 wt% and BNT-003 = 5.41 wt% as analyzed; LOI* and Total* are original LOI and oxide total as analyzed; N/A = data are not available.

[a] NASC = North American Shale Composite (Gromet et al., 1984).

[b] UCC = average Upper Continental Crust (Taylor and McLennan, 1985).

2002). The ratios between relatively immobile elements such as Th/Sc and Zr/Sc are good indicators of provenance. The studied samples have ratios comparable to average Proterozoic granite (Th/Sc = 3.6, Zr/Sc = 48 and Rb/Sr = 1.3, Condie, 1993) as compared with those of NASC and UCC (Gromet et al., 1984; Taylor and McLennan, 1985). Th/Sc–Zr/Sc diagram is a useful index of zircon enrichment (McLennan et al., 1993) (Fig. 14). Zircons accumulate during sedimentation while less resistant phases are preferentially destroyed. The Zr/Sc ratio is a useful tracer for zircon or heavy mineral concentration (Taylor and McLennan, 1985). In first-cycle sediments, Th/Sc ratios show an overall positive correlation with Zr/Sc, depending on the nature of the source rock. In contrast, Zr/Sc ratios

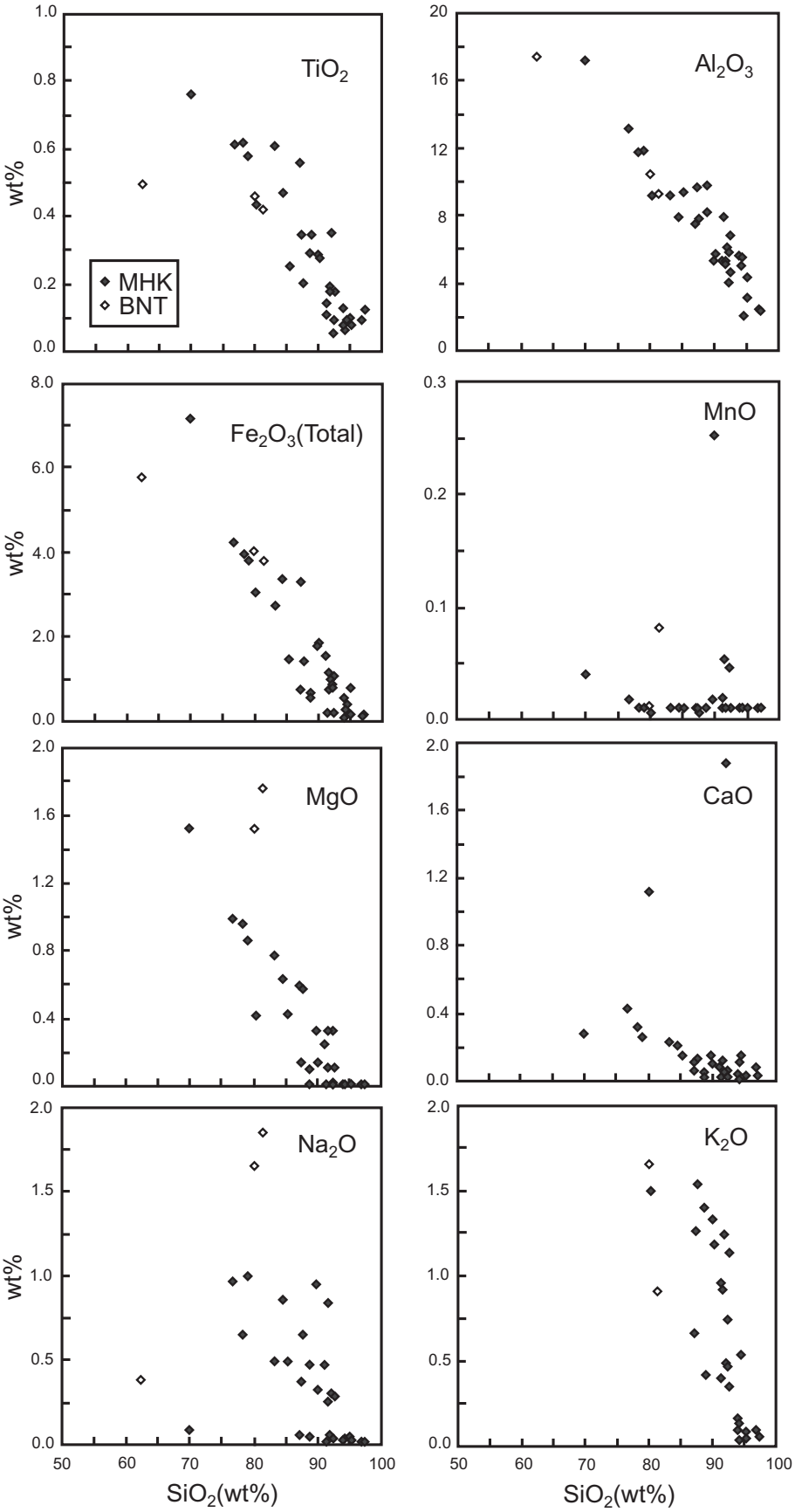

Fig. 6. Harker variation diagrams for Mo Hin Khao and Ban Non Toom sediments. Some data from Ban Non Toom with higher values are omitted for clarity. The decrease in the abundance of TiO_2, Al_2O_3, Fe_2O_3, MgO, Na_2O, and K_2O as the increase of SiO_2 content, indicates that the samples increase in mineralogical maturity.

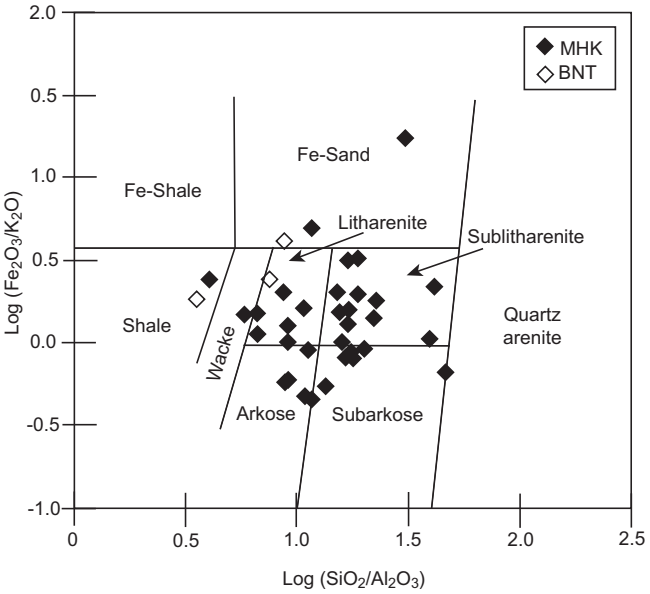

Fig. 7. Chemical classification of the Mo Hin Khao clastic rocks (fields after Herron (1988)). The samples fall mainly in litharenite and sublitharenite fields with some are in subarkose and arkose fields. This shows that they are mainly sandstone containing some lithic fragments, other than quartz and feldspar with some clayey matrix. The fields of arkose and subarkose reflect the present of feldspar.

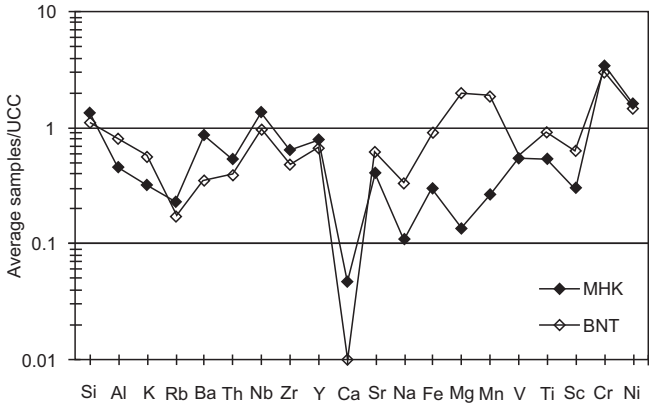

Fig. 9. Multi-element diagram for the average samples of Mo Hin Khao and Ban Non Toom normalized against average Upper Continental Crust (UCC) from Taylor and McLennan (1985). The elements are arranged according to those derived mainly from felsic source rocks on the left-hand side and those from mafic and ultramafic source rocks on the right-hand side. Note, Ca ratio for BNT equals zero due to excluded from the calculation. The average values for UCC can be found in Table 5.

in mature or recycled sediments display considerable variation with little change in the accompanying Th/Sc ratio (McLennan et al., 1993), indicating zircon addition due to sediment recycling (Fig. 14). Some lower values in the diagram show the simple correlation ratios and agree well with the compositional variation trend. This indicates lessened affect of sedimentary process, with the higher values from enrichments of zircon (high Zr/Sc ratio) resulting from sedimentary sorting and recycling. This pattern is attributed to compositional variations.

The high Th/Sc is not only due to the rocks' derivation from more felsic sources, but is also related to concentration of heavy minerals (e.g. zircon) during sedimentary recycling and sorting. The mineralogical maturity of the sediments, based on the proportion of compositionally mature alumina-rich minerals such as kaolinite, also is consistent with a felsic or a reworked sedimentary source (e.g. Cullers et al., 1975, 1987). Enrichments of normally incompatible over compatible elements, e.g. high Th/Sc, reflect relatively acidic average provenance compositions, and high Rb/Sr (>0.5) reflects weathering and sedimentary recycling (McLennan

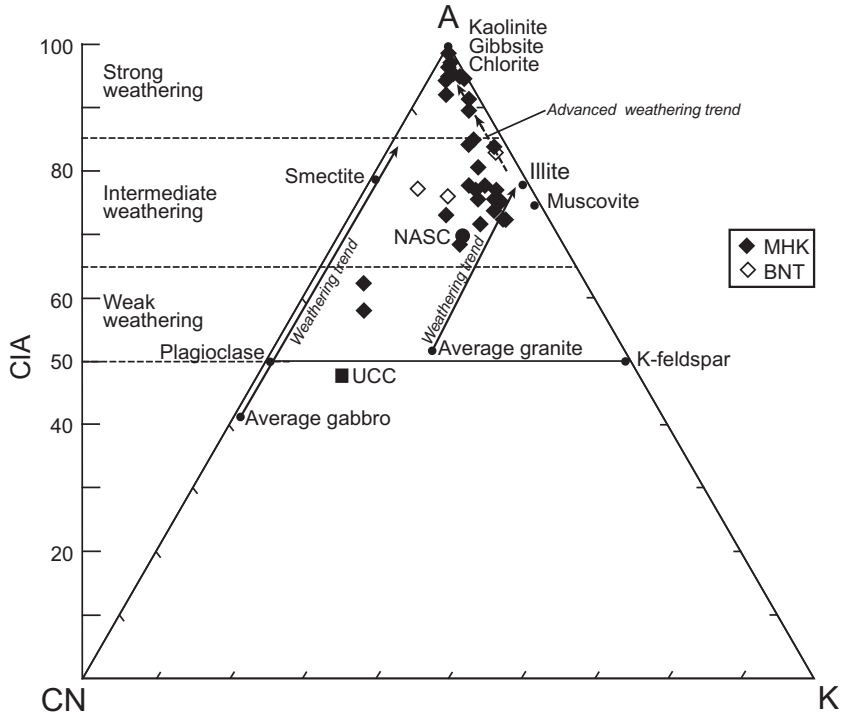

Fig. 8. Chemical Index of Alteration (CIA) with ternary diagram, A–CN–K (Al_2O_3–CaO^* + Na_2O–K_2O) (after Nesbitt and Young (1982, 1984, 1989)) of the samples from Mo Hin Khao and Ban Non Toom. UCC = average Upper Continental Crust from Taylor and McLennan (1985); NASC = North American Shale Composite from Gromet et al. (1984). Most studied sediments fall in the fields of intermediate and strong weathering which reflect the presence of mature sands containing relatively unfresh detrital feldspars and points to a relatively weathered or a tectonically inactive source.

Table 6
Correlation coefficient matrix of chemical elements in the samples.

	Al_2O_3	Fe_2O_3(T)	K_2O	MgO	MnO	Na_2O	P_2O_5	SiO_2	TiO_2	CaO	LOI	Ni	V	Rb	Y	Nb	Th	Cr	Sr	Ba	Sc	Zr
Al_2O_3	1.0																					
Fe_2O_3(T)	0.8	1.0																				
K_2O	0.78	0.8	1.0																			
MgO	0.4	0.6	0.4	1.0																		
MnO	0.0	0.1	0.0	0.4	1.0																	
Na_2O	0.3	0.4	0.4	0.2	0.0	1.0																
P_2O_5	−0.3	−0.1	−0.2	−0.1	−0.1	−0.1	1.0															
SiO_2	−0.5	−0.6	−0.5	−1.0	−0.4	−0.3	0.1	1.0														
TiO_2	0.83	0.9	0.81	0.4	0.0	0.4	−0.2	−0.5	1.0													
CaO	0.1	0.2	0.0	0.9	0.5	0.1	0.0	−0.9	0.0	1.0												
LOI	0.2	0.3	0.2	0.9	0.5	0.1	−0.1	−0.9	0.2	1.0	1.0											
Ni	0.6	0.8	0.7	0.2	0.4	0.2	−0.2	−0.3	0.8	−0.1	0.0	1.0										
V	0.8	0.9	0.8	0.3	−0.1	0.3	−0.2	−0.4	1.0	−0.1	0.1	0.7	1.0									
Rb	0.81	0.78	0.96	0.3	0.0	0.3	−0.2	−0.4	0.86	−0.1	0.1	0.8	0.8	1.0								
Y	0.4	0.6	0.4	−0.1	0.2	0.4	−0.3	0.0	0.6	−0.3	−0.2	0.8	0.6	0.6	1.0							
Nb	−0.6	−0.8	−0.8	−0.7	−0.4	−0.4	0.1	0.8	−0.7	−0.5	−0.6	−0.7	−0.6	−0.7	−0.5	1.0						
Th	−0.2	−0.1	−0.1	−0.5	−0.3	−0.1	0.0	0.5	0.0	−0.5	−0.5	0.1	0.1	0.0	0.4	0.3	1.0					
Cr	0.5	0.6	0.6	0.0	−0.1	0.4	0.0	0.0	0.8	−0.3	−0.2	0.7	0.8	0.6	0.7	−0.4	0.2	1.0				
Sr	0.2	0.2	0.1	0.6	0.4	0.2	−0.1	−0.7	0.1	0.7	0.7	0.0	0.1	0.1	−0.1	−0.4	−0.5	−0.3	1.0			
Ba	0.0	0.1	0.1	−0.1	0.77	0.1	−0.1	0.0	0.1	−0.1	−0.1	0.6	0.1	0.2	0.5	−0.3	0.0	0.2	0.1	1.0		
Sc	0.7	0.8	0.6	0.7	0.0	0.1	−0.1	−0.7	0.8	0.3	0.5	0.5	0.7	0.6	0.3	−0.6	0.0	0.4	0.3	0.0	1.0	
Zr	0.1	0.2	0.2	−0.2	−0.1	0.3	−0.2	0.1	0.5	−0.3	−0.2	0.3	0.5	0.3	0.6	0.0	0.3	0.6	0.0	0.2	0.2	1.0

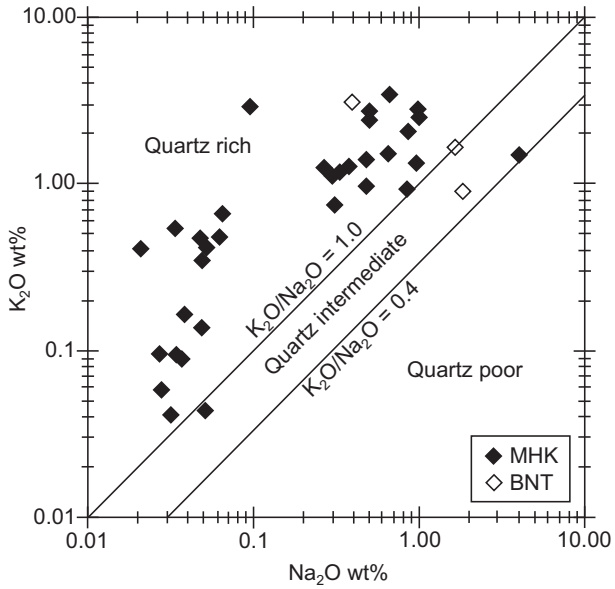

Fig. 10. Use of major elements for chemical classification, indicating the richness of quartz of the samples (Crook, 1974).

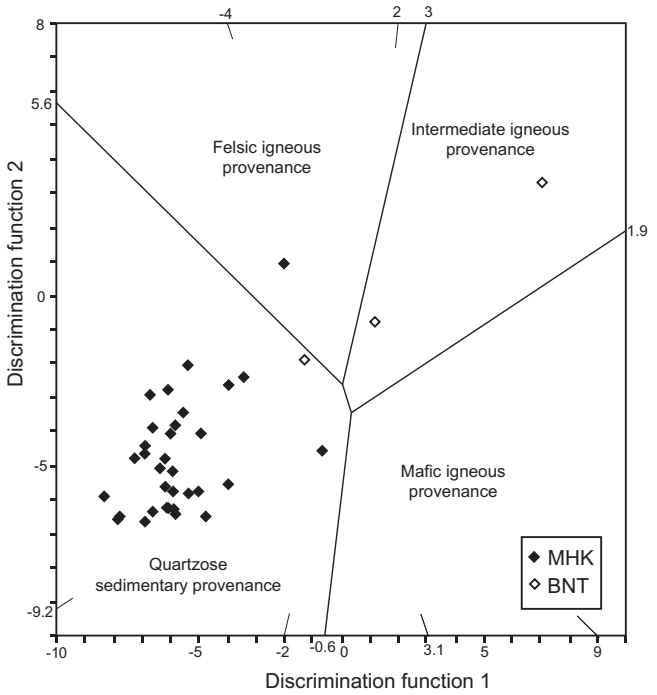

Fig. 11. Plot of discrimination functions 1 (=−1.773TiO_2 + 0.607Al_2O_3 + 0.76$Fe_2O_{3(tot)}$ − 1.5MgO + 0.616CaO + 0.509Na_2O − 1.224K_2O − 9.09) vs. 2 (=0.445TiO_2 + 0.07Al_2O_3 − 0.25$Fe_2O_{3(tot)}$ − 1.142MgO + 0.438CaO + 1.475Na_2O + 1.426K_2O − 6.861), after Roser and Korsch (1988). The studied sediments (n = 36) show that most samples fall in the field of quartzose sedimentary provenance, *i.e.* they are mature polycyclic quartzose detritus. The samples from Ban Non Toom are unreliable within this diagram due to the biogenic CaO included in the functions.

et al., 1993). For the studied sediments, Th/Sc is a good overall indicator of igneous chemical differentiation processes because Th is a typical incompatible element, whereas Sc is typically compatible in igneous systems.

5. Discussion

The chemistry indicates that the sediments of the Phra Wihan Formation were reworked. The potential sources were igneous rocks with high silica content e.g. granite, pegmatite, etc. while the plagioclase in the lower part may link into intermediate igneous rocks, e.g. granodiorite and diorite. The tourmaline could directly come from granitoid, aplite or pegmatite. These minerals could either derive from known very ancient igneous rocks or younger rocks crystallized just before the age of deposition, e.g. the Eastern Province Granitoids dated from Early Permian to Latest Triassic.

5.1. Tectonic settings

The studied samples exhibit high percentages of lithic fragments and matrix, high quartz content and presence of medium to well-sorted sub-round to sub-angular framework grains. These are features of compositionally mature sandstones. On the Q–F–L triangular diagram (Fig. 5), the samples plot around the corner of quartz and according to the fields in the similar diagram of Dickinson et al. (1983), and occupy the area of craton interior and the recycled orogenic. This may indicate possible mixing of

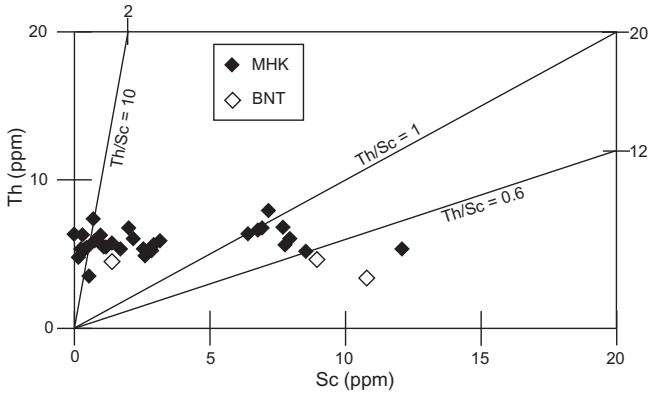

Fig. 12. Th vs. Sc for rock samples. Th/Sc = 1 ratio represents the average Upper Continental Crust (UCC) (data from Taylor and McLennan (1985)).

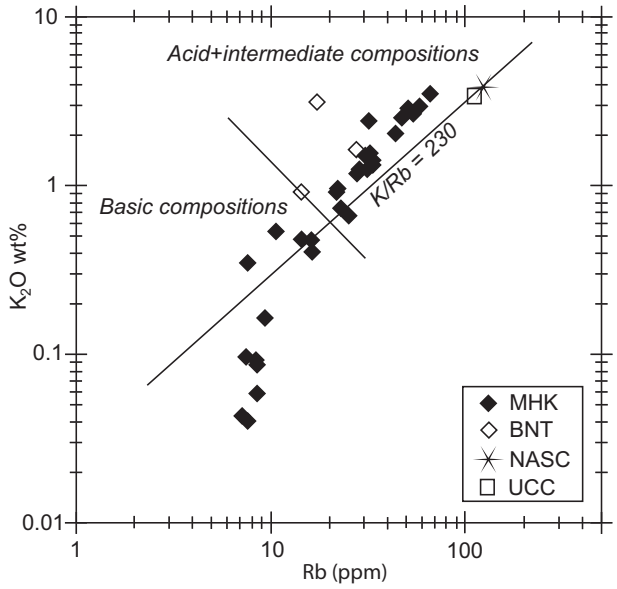

Fig. 13. Distribution of K and Rb in the samples relative to a K/Rb ratio of 230 (=main trend of Shaw (1968)). Overall the studied samples show sources of acid and intermediate origins and the rest are from basic rocks. NASC = North American Shale Composite from Gromet et al. (1984); UCC = average Upper Continental Crust from Taylor and McLennan (1985).

sediment from an eroded, mature continental island arc, passive margin and from quartzose recycled sources. The source rocks may be of two types: a continental source (responsible for the quartz fragments and the high resistant lithic chert grains) and a plutonic-arc source (responsible for the amounts of quartz, feldspar and plutonic accessory-mineral fragments).

Several classifications attempt to discriminate various origins and tectonic settings (Maynard et al., 1982; Bhatia, 1983; Bhatia and Crook, 1986; Roser and Korsch, 1986, 1988). Roser and Korsch (1986) used log (K_2O/Na_2O) vs. SiO_2 (Fig. 15) to determine the tectonic setting of the source of terrigenous sedimentary rocks. SiO_2 and K_2O/Na_2O increase from volcanic-arc to active continental margin to passive margin settings. Nearly all studied samples plot in the passive margin field, leaving only two in the active continental margin field. Roser and Korsch (1986), consider passive margin sediments are largely quartz-rich sediments derived from plate interiors or stable continental areas and deposited in stable intracratonic basins or on passive continental margins. Discrimination of tectonic settings using TiO_2 vs. Fe_2O_3 + MgO and Al_2O_3/SiO_2 vs. Fe_2O_3 + MgO plots (Fig. 16), proposed by Bhatia (1983), includes oceanic island arc, continental island arc, active continental margin

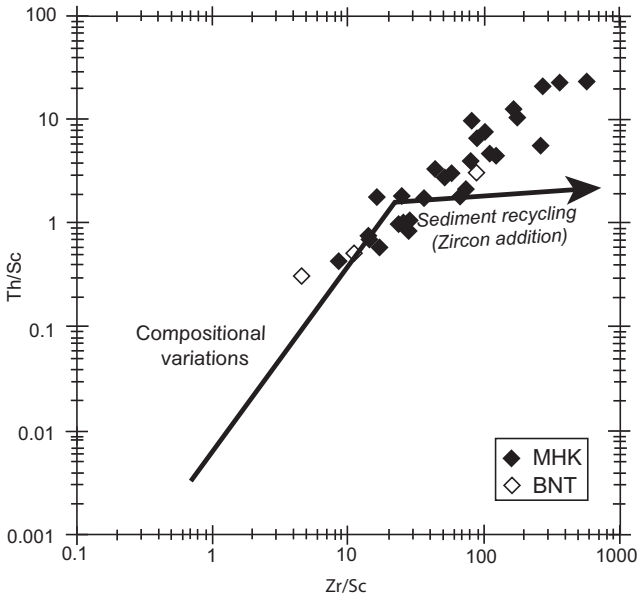

Fig. 14. Plot of Th/Sc vs. Zr/Sc for the samples (after McLennan et al. (1993)). The line in the lower part shows the compositional variation trend which indicates a reduced affect of sedimentary process. The arrowed line indicates the sediment recycling (zircon addition) or high Zr/Sc ratio resulting from sedimentary sorting and recycling.

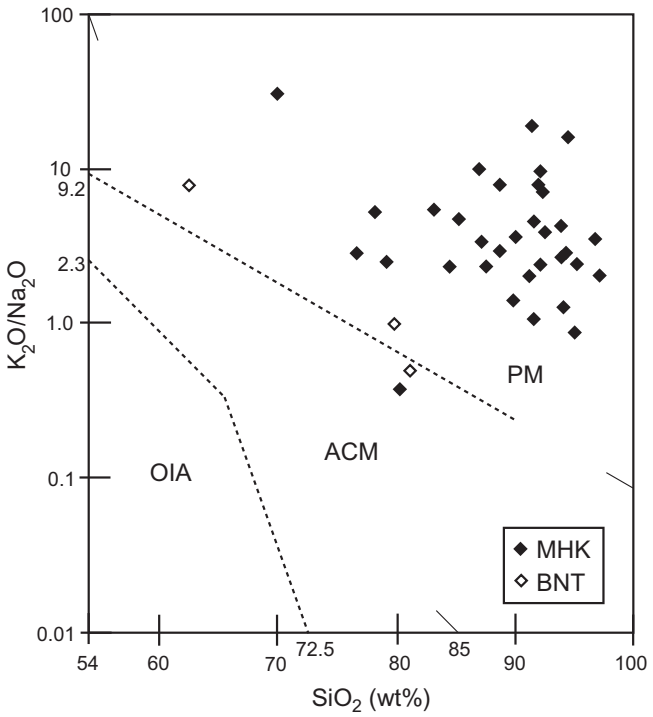

Fig. 15. SiO_2–K_2O/Na_2O diagram (Roser and Korsch, 1986) for Mo Hin Khao and Ban Non Toom sediments. The plot reveals the inferred tectonic setting (passive continental margin) of the source rocks from which the samples were derived. OIA = Oceanic island arc; ACM = Active continental margin; PM = Passive continental margin.

and passive margin settings. Most of the studied samples fall in/near the general area of PM = Passive margin and some samples are in ACM = Active continental margin. Few points fall outside these fields. Trace elements with low mobility and residence time in ocean water, e.g. La, Th, Zr and Sc, are transferred quantitatively into clastic sediments during primary weathering and transportation and are useful fingerprints for chemical discrimination of plate

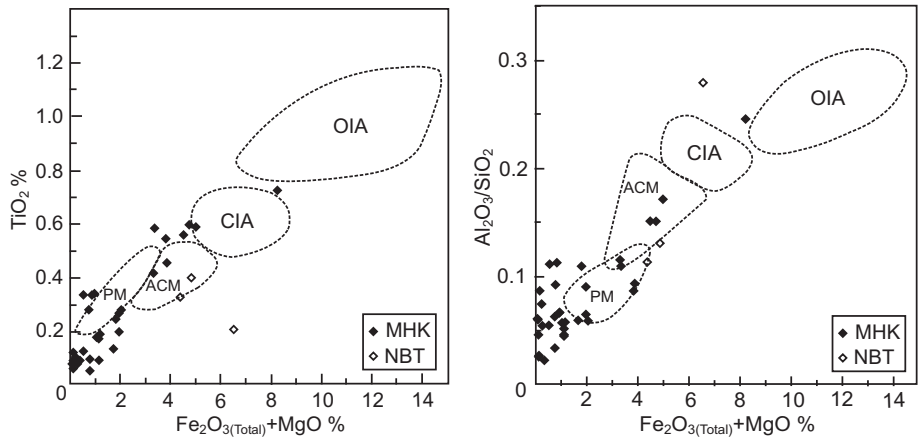

Fig. 16. Tectonic-setting discrimination diagrams for the studied sediments. Boundaries are after Bhatia (1983). OIA = Oceanic island arc; CIA = Continental island arc; ACM = Active continental margin; PM = Passive continental margin.

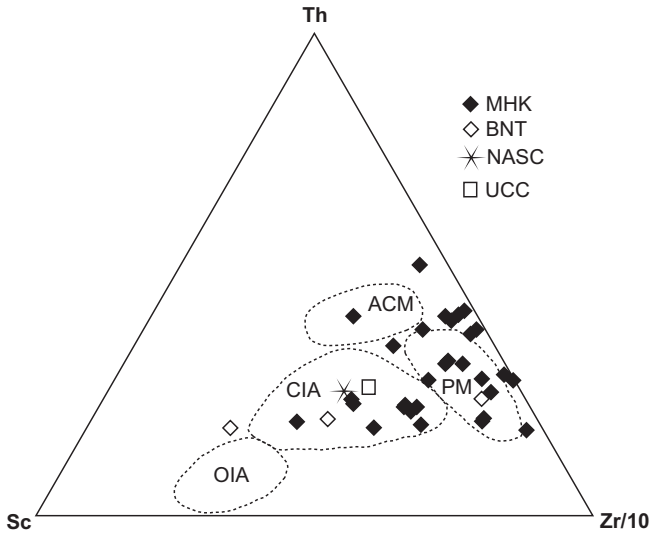

Fig. 17. Th–Sc–Zr/10 discriminatory plot of samples of this study, after Bhatia and Crook (1986). The fields represent various tectonic settings: OIA = Oceanic island arc; CIA = Continental island arc; ACM = Active continental margin; PM = Passive continental margins. UCC = average Upper Continental Crust from Taylor and McLennan (1985); NASC = North American Shale Composite from Gromet et al. (1984).

tectonic settings (Bhatia and Crook, 1986). The settings included: oceanic island arc (OIA), continental island arc (CIA), active continental margin (ACM) and passive margin (PM). In the discriminant ternary diagram, Th–Sc–Zr/10 of Bhatia and Crook (1986), the samples plot in the passive margin and continental island arc fields except for one in the active continental margin field (Fig. 17).

A clear explanation of passive and active continental margins is set out in Bhatia (1983). The passive margin tectonic setting comprises rifted continental margins; sedimentary basins on trailing continental margins supplied from collision orogens; and inactive or extinct convergent plate margins. The settings can be divided into prerift, rift-valley or graben and Atlantic-type continental trailing edges (Falvey, 1974; Maynard et al., 1982; Bhatia and Crook, 1986). The rift-valley or graben setting may apply to the studied area as the Khorat Basin developed as a series of major half-grabens in the Triassic extensional event. A collapse of the overthickened crust in this area, during the lndosinian Orogeny, led to thermal subsidence basin development later in the Early Cretaceous. The Jurassic and Cretaceous continental sediments of the Khorat Megasequence were deposited during the thermal subsidence phase which followed Triassic extension (Cooper et al., 1989). During the Jurassic marine sedimentation affected western Thailand, while a depositional hiatus characterized the Khorat Basin, then Late Jurassic and Early Cretaceous subsidence in a predominantly continental setting started in the Khorat Basin. The basin displays some minor marine incursions (e.g. Hahn, 1982; El Tabakh et al., 1999), so must have lain near sea level. Sedimentation presumably kept pace with subsidence and so deny more significant marine sedimentation. Basin development corresponded with active subduction and arc collision on the western margin of SE Asia, and active subduction on the Pacific margin (Morley, 2012). The closure of the back-arc basin (marked by the Jinghong–Nan–Sra Kaeo sutures) at about the end of Permian is correlated with the Early Triassic thermotectonism episode in Vietnam. Closure of the Palaeotethys Ocean, however, as Sibumasu collided with the continental Sukhothai Arc of Indochina, was later in the late Middle Triassic–early Late Triassic (post-Anisian), during the Indosinian Orogeny II (Sone and Metcalfe, 2008; Metcalfe, 2011a,b; Metcalfe, 2013). After that, the Khorat Basin became

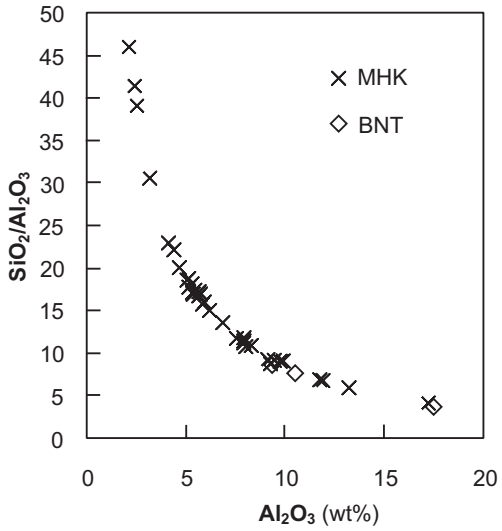

Fig. 18. The maturity index (SiO_2/Al_2O_3) plotted against Al_2O_3, showing that most samples have the index >5. The index indicates sediment maturation because values increase during weathering, transport and recycling, increasing modal framework of quartz over less resistant components, such as feldspar, pyriboles and lithic fragments (Roser et al., 1996).

relatively stable, supporting anastomosing river systems with a network of interconnected channels of various sinuosities and a random floodplain deposition (Horiuchi et al., 2012). Tectonic evolution of Khorat Basin area and SE Asia from middle Cretaceous to Palaeogene (Morley, 2012) suggests that the Region of transpressional deformation or inversion (uplift and erosion) and the synformal basin geometry probably arose from dynamic topography created by converging Tethyan and Palaeo-Pacific subduction zones. Extensive Palaeogene deformation and exhumation affected all margins of the Khorat Plateau. Deformation included folds of the Phu Phan uplift, and strike–slip faults, thrusts and folds on the southern and eastern margins. South of the Khorat Plateau outcrop, seismic data indicates syn-depositional fault-controlled subsidence was significant during Cretaceous deposition.

Although the rifting in the Khorat Basin was active and widespread during deposition of the Triassic whereas Booth and Sattayarak (2011) suggested that the younger succession including the Phra Wihan Formation was deposited in essentially a layer-cake fashion, accompanied by only local faulting (Ridd and Morley, 2011). Certain studies suggested that the Phra Wihan Formation was deposited in craton-interior setting or intracontinental basin (e.g. Racey, 2009). From the above evidence as well as petrographical and geochemical results of this study, it can be concluded that the sediment source may comprise of rocks originally formed in and later transported from the source terrains which had a mature continental island arc or a passive margin tectonic setting.

5.2. Weathering in the source areas

The Chemical Index of Altration (CIA) diagram (Fig. 8) is a good measure of degree of chemical weathering history from the source area (Nesbitt and Young, 1982; Nyakairu and Koeberl, 2001). It also records the progressive alteration of plagioclase and potassium feldspars to clay minerals. In general, intensive chemical weathering results in residual clays such as kaolinite and gibbsite, with CIA values 76–100. CIA values in shales range between ~65 and ~75, reflecting muscovite, illite and smectite compositions and indicate a moderately weathered source; between ~50 and ~65 indicate weak weathering. Fresh igneous rocks and feldspar have average CIA values of ~50 or ⩽50 indicating unweathered source areas (Nesbitt and Young, 1982).

The CIA values for the studied rocks vary across a wide range from 47 to 98 with an average of 78 (Table 5), indicating low to high weathering of the source areas. Only two samples fall in the weak weathering area (CIA = 58 and 63 in the plot, Fig. 8), which probably reflects the presence of immature sands containing relatively fresh detrital feldspars and point to a relatively unweathered source. Most data fall in the fields of intermediate and strong weathering (cf. Shao et al., 2012), reflecting the presence of mature sands containing relatively unfresh detrital feldspars from a relatively weathered or a tectonically inactive source. The data spread suggests the sediments could come from different chemical weathering sources.

The CIA values of the studied sediments point towards a more felsic source and may indicate sediment recycling processes (Nesbitt et al., 1980). Certain plots approached high Al_2O_3 contents above the average shales (NASC), so that a relatively high intensity of weathering may have proceeded to significant stripping of the alkali and alkali earth elements from the sediments. The high CIA values in the sediments probably stems from the presence of clay minerals and absence of detrital feldspars (Nyakairu and Koeberl, 2001). Albite found in a few samples, indicates remaining immaturity or weathering after deposition for the exposure beds. According to McLennan (1993), a CIA of 100 signifies wholesale removal of all alkali earths. Most CIA values for our study fall a little away from the illite and kaolinite, gibbsite and chlorite. The plagioclase in our samples (<1%) may imply insignificant chemical weathering during sedimentation in the basin. Alternatively, small amounts of feldspar in our samples as well as illite (Rahman and Faupl, 2003a,b) imply that the minerals are predominantly detrital and reflect the character of their source material (Weaver, 1958). The interbedded sandstones and mudrocks in the study area may reflect rapid erosion of fast rising orogens (cf. Rahman and Suzuki, 2007). Integrating the CIA values of both sandstones and mudrocks, favors the sediments of Mo Hin Khao as products of different zones of weathering in the sources.

According to Roser et al. (1996), the average maturity index (Fig. 18) is higher than 5, so that the sediments can be classed as mature, with possible reworking/recycling.

The lithic fragments are mainly chert, a common rock in MHK area. Highly resistant chert is widespread in Thailand and beyond as nodules in limestone and as beds in ocean floor deposits. The palaeoclimate of the deposition was probably tropical and the sediment of Phra Wihan Formation is more fractionated than the older formations. The plagioclase (albite) in the lower Formation (Phu Kradung Formation) can be explained lesser exposure, or less weathering, as normally the plagioclase is less resistant than alkali feldspar. According to Tucker (2001: 45), plagioclase feldspar is always found in sandstone sourced from uplifted oceanic and island-arc terrains. However, K_2O in most samples exceeds Na_2O, indicating the dominant role of clay content in the samples rather than plagioclase composition.

6. Conclusions

Petrography, mineralogy and geochemistry of Cretaceous sediment samples of Mo Hin Khao at the western margin of the Khorat Plateau, Thailand can contribute to their provenance study. Although the samples indicate significant weathering on CIA values, the geochemical and mineralogical results assist in characterizing the source rocks, as follows:

(1) Modal analysis suggests sediments input mainly from sedimentary and igneous (most likely plutonic) sources. The latter source would provide the feldspars and heavy minerals, e.g. zircon, tourmaline, amphiboles. Igneous rock source seems to consist of mainly felsic plutonic granite, pegmatite and intermediate rocks. Chert fragments indicate a possible sedimentary source area composed of uplifted chert beds and chert-bearing shale or limestone. Some highly resistant minerals such as quartz and zircon may be reworked from the lower formations of the Khorat Group, e.g. from Nam Phong to Phu Kradung.
(2) Most rocks at Mo Hin Khao are litharenite and sublitharenite with some being subarkose and arkose. The Q–F–L plots could cause confusion due to feldspar–quartz estimation, which can be solved by geochemistry.
(3) The mineral geochemistry indicates felsic to intermediate source rocks or possible mixing between felsic and basic source rocks.
(4) The source sediments and rocks could originate in and transported from a passive continental margin. However, the Phra Wihan Formation was deposited in an intracratonic environment with meandering, braided and anastomosing drainage on a large floodplain. Deposition in many sequences, produced thick clastic strata.
(5) The high silica content and maturity index indicates that the sediments of the areas are affected by reworking/recycling.

However, a relatively small data set and conclusions from this study based on heavy minerals is still incomplete. More Electron

Probe Microanalysis (EPMA), dating on detrital minerals are needed for further resolution.

Acknowledgements

We would like to offer our special thanks to the Thailand Research Fund (TRF) for financial support, and to Michael F. Ridd and Ian Metcalfe for helpful reviews. We are particularly grateful for assistance given by Federick Lin Sutherland and Pual Carling. Other much appreciated support came from Thaveesak Wongsricha (Assistant Director of Chaiyaphum Office of Tourism and Sports), for helping access to sites, make contacts and provide a field-trip assistant team, Buakhao Artnafai (Head of the Park rangers), Ranthom Soonsanthia, Phaitoon Samiphet, (a Park ranger), Juan Nongsra and his wife (Cham). Thanks also due to Ronald Stafan and Kamalaporn Kanongdate for proof reading the manuscript. Many people to whom we are indebted include Montri Kamnerdlom (Head of Phulaenkha National Park), Supitcha Supansomboon for literature searches, internship students from Mahasarakham University and other anonymous persons.

Appendix A. Supplementary material

Supplementary data associated with this article can be found, in the online version, at http://dx.doi.org/10.1016/j.jseaes.2014.01.007.

References

Ahrens, L.H., Erlank, A.J., 1969. Hafnium. In: Wedepohl, K.H. (Ed.), Handbook of Geochemistry, vol 2, part 5. Springer-Verlag, Berlin, sections B–O.

Bhatia, M.R., 1983. Plate tectonics and geochemical composition of sandstones. J. Geol. 91, 611–627.

Bhatia, M.R., Crook, K.A.W., 1986. Trace element characteristics of graywackes and tectonic setting discrimination of sedimentary basins. Contrib. Miner. Petrol. 92, 181–193.

Booth, J., Sattayarak, N., 2011. Subsurface Carboniferous–Cretaceous geology of NE Thailand. In: Ridd, M.F., Barber, A.J., Crow, M.J. (Eds.), The Geology of Thailand. Geological Society, London, pp. 185–222.

Buffetaut, E., Suteethorn, V., 1992. A new species of theornithischian dinosaur Psittacosaurus from the Early Cretaceous of Thailand. Palaeontology 35, 801–812.

Buffetaut, E., Suteethorn, V., Cuny, G., Tong, H., Le-Loeuff, J., Khansubha, S., Jongautchariyakul, S., 2000. The earliest known sauropod dinosaur. Nature 407, 72–74.

Carter, A., Bristow, C.S., 2003. Linking hinterland evolution and continental basin sedimentation by using detrital zircon thermochronology: a study of the Khorat Plateau Basin, eastern Thailand. Basin Res. 15, 271–285.

Chonglakmani, C., 2011. Triassic. In: Ridd, M.F., Barber, A.J., Crow, M.J. (Eds.), The Geology of Thailand. Geological Society, London, pp. 137–150.

Concepcion, R.A.B., Dimalanta, C.B., Yumul Jr., G.P., Faustino-Eslava, D.V., Queano, K.L., Tamayo Jr., R.A., Imai, A., 2012. Petrography, geochemistry and tectonics of a rifted fragment of Mainland Asia: evidence from the Lasala Formation, Mindoro Island, Philippines. Geol. Rundsch. 101, 273–290.

Condie, K.C., 1993. Chemical composition and evolution of the upper continental crust: contrasting results from surface samples and shales. Chem. Geol. 104, 1–37.

Cooper, M.A., Herbert, R., Hill, G.S., 1989. The structural evolution of Triassic intermontane basins in northeastern Thailand. In: Thanasuthipitak, T. (Ed.), International Symposium on Intermontane Basins: Geology & Resources. Chiang Mai, Thailand, pp. 231–242.

Cox, R., Lowe, D.R., Cullers, R.L., 1995. The influence of sediment recycling and basement composition on evolution of mudrock chemistry in south western United States. Geochim. Cosmochim. Acta 59, 2919–2940.

Crook, K.A.W., 1974. Lithostratigraty and geotectonic: the significance of composition variation in Flysch arenites (graywakes). In: Dott, R.H., Shaver, R.H. (Eds.), Modern and Ancient Geosynclinal Sedimentation. Society of Economic Paleontologists and Mineralogists, Tulsa, Okla, USA, pp. 304–310 (Special Publications).

Cullers, R.L., 1988. Mineralogical and chemical changes of soil and stream sediment formed by intense weathering of the Danburg granite, Georgia, USA. Lithos 21, 301–314.

Cullers, R.L., 1994. The controls on the major and trace element variation of shales, siltstones and sandstones of Pennsylvanian–Permian age from uplifted continental blocks in Colorado to platform sediment in Kansas, USA. Geochim. Cosmochim. Acta 58, 4955–4972.

Cullers, R.L., 1995. The controls on the major- and trace-element evolution of shales, siltstones and sandstones of Ordovician to Tertiary age in wet mountains region, Colorado, USA. Chem. Geol. 123, 107–131.

Cullers, R.L., 2000. The geochemistry of shales, siltstones and sandstones of Pennsylvanian–Permian age, Colorado, USA: Implications for provenance and metamorphic studies. Lithos 51, 181–203.

Cullers, R.L., Podkovyrov, V.N., 2000. Geochemistry of the Mesoproterozoic Lakhanda shales in southeastern Yakutia, Russia: implications for mineralogical and provenance control and recycling. Precambr. Res. 104, 77–93.

Cullers, R.L., Podkovyrov, V.N., 2002. The source and origin of terrigenous sedimentary rocks in the Mesoproterozoic Ui Group, south-eastern Russia. Precambr. Res. 117, 157–183.

Cullers, R.L., Chaudhuri, S., Arnold, B., Lee, M., Wolf, C.W., 1975. Rare earth distributions in clay minerals and in clay-sized fraction of the lower Permian Havensville and Eskridge shales of Kansas and Oklahoma. Geochim. Cosmochim. Acta 39, 1691–1703.

Cullers, R.L., Barrett, T., Carlson, R., Robinson, B., 1987. Rare-Earth element and mineralogic changes in Holocene soil and stream sediment: a case study in the wet mountains region, Colorado, USA. Chem. Geol. 63, 275–297.

Cullers, R.L., Basu, A., Suttner, L.J., 1988. Geochemical signature of provenance in sand-size material in soils and stream sediments near the Tobacco Root batholith, Montana, USA. Chem. Geol. 70, 335–348.

Dabard, M.P., 1990. Lower Brioverian formations (Upper Proterozoic) of the Armorican Massif (France): geodynamic evolution of source areas revealed by sandstone petrography and geochemistry. Sed. Geol. 69, 45–58.

Deer, W.A., Howie, R.A., Zussman, J., 1996. An Introduction to the Rock-forming Minerals, second ed. Addison Wesley Longman Limited, Edinburgh, 696p.

Department of Mineral Resources, 2007. Geological Map of Chaiyaphum. <http://www.dmr.go.th/ewtadmin/ewt/dmr_web/main.php?filename=Regist_geo_province_En> (accessed on 30.10.12).

Dickinson, W.R., Beard, L.S., Brakenridge, G.R., Erjavec, J.L., Ferguson, R.C., Inman, K.F., Knepp, R.A., Lindberg, F.A., Ryberg, P.T., 1983. Provenance of North American Phanerozoic sandstones in relation to tectonic setting. Geol. Soc. Am. Mem. 94, 222–235.

Diskin, S., Evans, J., Fowler, M.B., Guion, P.D., 2011. Recognising different sediment provenances within a passive continental margin setting: towards characterising a sediment source to the west of the British late Carboniferous sedimentary basins. Chem. Geol. 283, 143–160.

Droop, G.T.R., 1987. A general equation for estimating Fe^{3+} concentrations in ferromagnesian silicates and oxides from microprobe analyses, using stoichiometric criteria. Mineral. Mag. 51, 431–435.

El Tabakh, M., Utha-Aroon, C., Schreiber, B.C., 1999. Sedimentology of the Cretaceous Maha Sarakham evaporites in the Khorat Plateau of northeastern Thailand. Sed. Geol. 123, 31–62.

Falvey, D.A., 1974. The development of continental margins in plate tectonic theory. Aust. Petrol. Explor. Assoc. 14, 95–106.

Fedo, C.M., Nesbitt, H.W., Young, G.M., 1995. Unravelling the effects of potassium metasomatism in sedimentary rocks and paleosols, with implications for paleoweathering conditions and provenance. Geology 23, 921–924.

Feng, R., Kerrich, R., 1990. Geochemistry of finegrained clastic sediments in the Archean Abitibi greenstones belt, Canada: implications for provenance and tectonic setting. Geochim. Cosmochim. Acta 54, 1061–1081.

Garver, J.I., Royce, P.R., Smick, T.A., 1996. Chromium and nickel in shale of the Taconic Foreland: a case study for the provenance of fine-grained sediments with an ultramafic source. J. Sediment. Res. 66, 100–106.

Ghandour, I.M., Harue, M., Wataru, M., 2003. Mineralogical and chemical characteristics of Bajocian-Bathonian shales, G. Al-Maghara, North Sinai, Egypt: Climatic and environmental significance. Geochem. J. 37, 87–108.

Gromet, L.P., Dymek, R.F., Haskin, L.A., Korotev, R.L., 1984. The 'North American Shale Composite': its compilation, major and trace element characteristics. Geochim. Cosmochim. Acta 48, 2469–2482.

Hahn, L., 1982. Stratigraphy and marine ingression of the Mesozoic Khorat Group in northeastern Thailand. Geol. Jahrb. 43, 7–35.

Henry, D.J., Guidotti, C.V., 1985. Tourmaline as a petrogenetic indicator mineral: an example from the staurolite-grade metapelites of NW Maine. Am. Mineral. 70, 1–15.

Herron, M.M., 1988. Geochemical classification of terrigeneous sands and shales from core or log data. J. Sediment. Petrol. 58, 820–829.

Holland, H.D., 1978. The Chemistry of the Atmosphere and the Oceans. John Wiley & Sons Inc., New York, 351p.

Horiuchi, Y., Charusiri, P., Hisada, K., 2012. Identification of an anastomosing river system in the Early Cretaceous Khorat Basin, northeastern Thailand, using stratigraphy and paleosols. J. SE Asian Earth Sci. 61, 62–77.

Leake, B.E., Woolley, A.R., Arps, E.E.S., Birch, W.D., Gilbert, M.E., Grice, J.D., Hawthorne, F.E., Kato, A., Kisch, H.J., Krivovichev, V.G., Linthout, K., Laird, J., Mandarino, J., Maresch, W.V., Nickel, E.H., Rock, N.M.S., Schumacher, J.E., Smith, D.E., Stephenson, N.C.N., Ungaretti, L., Whittaker, E.J.W., Youzhi, G., 1997. Nomenclature of amphiboles: report of the subcommittee on amphiboles of the international mineralogical association, commission on new minerals and mineral names. Can. Mineral. 35, 219–246.

Lertsirivorakul, R., Sompadung, S., Hirunkerd, W., 2006. Geotourism Resource Investigation. Final Report No. 3 of Sustainable Ecotourism Promotion of Mo Hin Khao Project. Research Center for Mekong Regional Tourism (ReCMeRT) Khon Kaen University (KKU), pp. 207–248 (In Thai).

Malila, K., Chonglakmani, C., Qinglai, F., Helmcke, D., 2008. Provenance and tectonic setting of the Permian Nam Duk Formation, North – Central Thailand: implications for geodynamic evolution. Sci. Asia 34, 007–022.

Mange, M.A., Morton, A.C., 2007. Geochemistry of heavy minerals. In: Mange, M.A., Wright, D.T. (Eds.), Heavy Minerals in Use. Developments in Sedimentology, vol. 58, pp. 345–391.

Maynard, J.B., Valloni, R., Yu, H.S., 1982. Composition of modern deep-sea sands from arc-related basins. In: Leggett, J.K. (Ed.), Trench and Fore-arc Sedimentation. The Geological Society of London, pp. 551–561 (Special Publications 10).

McLennan, S.M., 1989. Rare earth elements in sedimentary rocks: influence of provenance and sedimentary processes. In: Lipin, B.R., McKay, G.A. (Eds.), Geochemistry and Mineralogy of Rare Earth Elements. Reviews in Mineralogy and Geochemistry, vol. 21. Mineralogical Society of America, pp. 169–200.

McLennan, S.M., 1993. Weathering and global denudation. J. Geol. 101, 295–303.

McLennan, S.M., Taylor, S.R., 1991. Sedimentary rocks and crustal evolution: tectonic setting and secular trends. J. Geol. 99, 1–21.

McLennan, S.M., Nance, W.B., Taylor, S.R., 1980. Rare earth element-thorium correlations in sedimentary rocks and the composition of the continental crust. Geochim. Cosmochim. Acta 44, 1833–1839.

McLennan, S.M., Taylor, S.R., Kröner, A., 1983. Geochemical evolution of Archean shales from South Africa I. The Swaziland and Pongola Supergroups. Precambr. Res. 22, 93–124.

McLennan, S.M., Hemming, S., McDaniel, D.K., Hanson, G.N., 1993. Geochemical approaches to sedimentation, provenance and tectonics. In: Johnson, M.J., Basu, A. (Eds.), Processes Controlling the Composition of Clastic Sediments. The Geological Society of America, pp. 21–40 (Special Paper 284).

Meesook, A., 2000. Cretaceous environments of Northeastern Thailand. In: Okada, H., Mateer, N.J. (Eds.), Cretaceous Environments of Asia. Elsevier, Amsterdam, pp. 207–223.

Meesook, A., 2011. Cretaceous. In: Ridd, M.F., Barber, A.J., Crow, M.J. (Eds.), The Geology of Thailand. The Geological Society of London, pp. 169–184.

Meesook, A., Saengsrichan, W., 2011. Jurassic. In: Ridd, M.F., Barber, A.J., Crow, M.J. (Eds.), The Geology of Thailand. The Geological Society of London, pp. 151–168.

Meesook, A., Suteethorn, V., Chaodamrong, P., Teerarungsigul, N., Sardsud, A., Wongprayoon, T., 2002. Mesozoic rocks of Thailand: a summary. In: Mantajit, N. (Ed.), Proceedings of the Symposium on Geology of Thailand, Bangkok, Thailand, pp. 82–94.

Metcalfe, I., 2011a. Palaeozoic–Mesozoic history of SE Asia. In: Hall, R., Cottam, M., Wilson, M. (Eds.), The SE Asian Gateway: History and Tectonics of Australia–Asia Collision, vol. 355. Geological Society of London Special Publications, pp. 7–35.

Metcalfe, I., 2011b. Tectonic framework and Phanerozoic evolution of Sundaland. Gondwana Res. 19, 3–21.

Metcalfe, I., 2013. Gondwana dispersion and Asian accretion: tectonic and palaeogeographic evolution of eastern Tethys. J. Asian Earth Sci. 66, 1–33.

Mishra, M., Sen, S., 2012. Provenance, tectonic setting and source-area weathering of Mesoproterozoic Kaimur Group, Vindhyan Supergroup, Central India. Geol. Acta 10, 283–293.

Morley, C.K., 2012. Late Cretaceous-Early Palaeogene tectonic development of SE Asia. Earth Sci. Rev. 115, 37–75.

Morton, A.C., 1991. Geochemical studies of detrital heavy minerals and their application to provenance research. In: Morton, A.C., Todd, S.P., Haughton, P.D.W. (Eds.), Developments in Sedimentary Provenance Studies. The Geological Society of London, pp. 31–45 (Special Publications 57).

Morton, A.C., Hallsworth, C.R., 1994. Identifying provenance-specific features of detrital heavy mineral assemblages in sandstones. Sed. Geol. 90, 241–256.

Morton, A.C., Hallsworth, C.R., 1999. Processes controlling the composition of heavy mineral assemblages in sandstones. Sed. Geol. 124, 3–29.

Morton, A.C., Hallsworth, C.R., 2007. Stability of detrital heavy minerals during burial diagenesis. In: Mange, M., Wright, D.K. (Eds.), Heavy Minerals in US. Developments in Sedimentology, vol. 58, pp. 215–245.

Nesbitt, H.W., Young, G.M., 1982. Early Proterozoic climates and plate motions inferred from major element chemistry of lutite. Nature 299, 715–717.

Nesbitt, H.W., Young, G.M., 1984. Prediction of some weathering trends of plutonic and volcanic rocks based on thermodynamic and kinetic considerations. Geochim. Cosmochim. Acta 48, 1523–1534.

Nesbitt, H.W., Young, G.M., 1989. Formation and diagenesis of weathering profiles. J. Geol. 97, 129–147.

Nesbitt, H.W., Markovics, G., Price, R.C., 1980. Chemical processes affecting alkalis and alkali earths during continental weathering. Geochim. Cosmochim. Acta 44, 1659–1666.

Nyakairu, G.W.A., Koeberl, V., 2001. Mineralogical and chemical composition and distribution of rare earth elements in clay-rich sediments from central Uganda. Geochem. J. 35, 13–28.

Owen, M.R., 1987. Hafnium content of detrital zircons, a new tool for provenance study. J. Sediment. Petrol. 57, 824–830.

Pettijohn, F.J., Potter, P.E., Siever, R., 1987. Sand and sandstone, second ed. Springer-Verlag, New York, 553p.

Racey, A., 2009. Mesozoic red bed sequences from SE Asia and the significance of the Khorat Group of NE Thailand. In: Buffetaut, E., Cuny, G., Le Loeuff, J., Suteethorn, V. (Eds.), Late Palaeozoic and Mesozoic Ecosystems in SE Asia. The Geological Society of London, pp. 41–67 (Special Publications 315).

Racey, A., Goodall, J.G.S., 2009. Palynology and stratigraphy of the Mesozoic Khorat Group red bed sequences from Thialnd. In: Buffetaut, E., Cuny, G., Le Loeuff, J., Suteethorn, V. (Eds.), Late Palaeozoic and Mesozoic Ecosystems in SE Asia. The Geological Society of London, pp. 69–83 (Special Publications 315).

Racey, A., Love, M.A., Canham, A.C., Goodall, J.G.S., Polachan, S., Jones, P.D., 1996. Stratigraphy and reservoir potential of the Mesozoic Khorat Group, NE Thailand: Part 1: Stratigraphy and sedimentary evolution. J. Pet. Geol 19, 5–39.

Rahman, M.J.J., Faupl, P., 2003a. The composition of the subsurface Neogene shales of the Surma Group from the Sylhet Trough, Bengal Basin, Bangladesh. In: Alam, M.M., Curray, J.R. (Eds.), Sedimentary Geology of the Bengal Basin, Bangladesh, In Relation to the Asia–Greater India Collision and the Evolution of the Eastern Bay of Bengal. Sedimentary Geology, vol. 155. Elsevier Science, pp. 407–417.

Rahman, M.J.J., Faupl, P., 2003b. $^{40}Ar/^{39}Ar$ multigrain dating of detrital white mica of sandstones of the Surma Group in the Sylhet Trough, Bengal Basin, Bangladesh. In: Alam, M.M., Curray, J.R. (Eds.), Sedimentary Geology of the Bengal Basin, Bangladesh, In Relation to the Asia–Greater India Collision and the Evolution of the Eastern Bay of Bengal. Sedimentary Geology, vol. 155. Elsevier Science, pp. 383–392.

Rahman, M.J.J., Suzuki, S., 2007. Geochemistry of sandstones from the Miocene Surma Group, Bengal Basin, Bangladesh: implications for Provenance, tectonic setting and weathering. Geochem. J. 41, 415–428.

Ridd, M.F., Morley, C.K., 2011. The Khao Yai Fault on the southern margin of the Khorat Plateau, and the pattern of faulting in Southeast Thailand. Proc. Geol. Assoc. 122, 143–156.

Roser, B.P., Korsch, R.J., 1986. Determination of tectonic setting of sandstone–mudstone suites using SiO_2 content and K_2O/Na_2O ratio. J. Geol. 94, 635–650.

Roser, B.P., Korsch, R.J., 1988. Provenance signatures of sandstone–mudstone suites determined using discriminant function analysis of major-element data. Chem. Geol. 67, 119–139.

Roser, B.P., Cooper, R.A., Nathan, S., Tulloch, A.J., 1996. Reconnaissance sandstone geochemistry, provenance and tectonic setting of the lower Paleozoic terranes of the West Coast and Nelson, New Zealand. NZ J. Geol. Geophys. 39, 1–16.

Sattayarak, N., 1985. Review on geology of Khorat Plateau: In: Phiancharoen, C. (Ed.), Proceedings on Geology and Mineral Resources Development of the Northeast, Thailand. Khon Kaen, pp. 23–30 (in Thai).

Shao, J., Yang, S., Li, C., 2012. Chemical indices (CIA and WIP) as proxies for integrated chemical weathering in China: inferences from analysis of fluvial sediments. Sed. Geol. 265–266, 110–120.

Shaw, D.M., 1968. A review of K–Rb fractionation trends by covariance analysis. Geochim. Cosmochim. Acta 32, 573–602.

Sone, M., Metcalfe, I., 2008. Parallel Tethyan sutures in mainland Southeast Asia: New insights for Palaeo-Tethys closure and implications for the Indosinian orogeny. C.R. Geosci. 340, 166–179.

Taylor, S.R., McLennan, S.H., 1985. The Continental Crust: Its Composition and Evolution. Blackwell, Oxford, 312p.

Tindle, A., 2012. Probe–Amph 3.0 (in Excel Format). <http://www.open.ac.uk/earth-research/tindle/AGT/AGT_ Home_2010/Microprobe-2.html> (aceeses on 13.07.12).

Tucker, M.E., 2001. Sedimentary Petrology, third ed. Blackwell Science, Oxford, 262p.

Wang, X., Griffin, W.L., Chen, J., 2010. Hf contents and Zr/Hf ratios in granitic zircons. Geochem. J. 44, 65–72.

Weaver, C.E., 1958. Geologic interpretation of argillaceous sediments. Part 1. Origin and significance of clay minerals in sedimentary rocks. Am. Assoc. Pet. Geol. Bull. 42, 254–271.

Weber, J.N., Middleton, G.V., 1961a. Geochemistry of the turbidites of the Nornanskill and Charney formations-I: effect of turbidity currents on chemical differentiation of turbidites. Geochim. Cosmochim. Acta 22, 200–243.

Weber, J.N., Middleton, G.V., 1961b. Geochemistry of the turbidites of the Normanskill and Charney formations-II: distribution of trace elements. Geochim. Cosmochim. Acta 22, 244–288.

Wronkiewicz, D.J., Condie, K.C., 1987. Geochemistry of Archean shales from the Witwatersrand Supergroup South Africa: source-area weathering and provenance. Geochim. Cosmochim. Acta 51, 2401–2416.

Wronkiewicz, D.J., Condie, K.C., 1989. Geochemistry and provenance of sediments from the Pongola Supergroup, South Africa: evidence for a 3.0 Ga old continental craton. Geochim. Cosmochim. Acta 53, 1537–1549.

Wronkiewicz, D.J., Condie, K.C., 1990. Geochemistry and mineralogy of sediments from the Ventersdorp and Transvaal Supergroups, South Africa: cratonic evolution during the early Proterozoic. Geochim. Cosmochim. Acta 54, 343–354.

Yan, Y., Xia, B., Lin, G., Cui, X., Hu, X., Yan, P., Zhang, F., 2007. Geochemistry of the sedimentary rocks from the Nanxiong Basin, South China and implications for the provenance, paleoenvironment and paleoclimate at the K/T boundary. Sed. Geol. 197, 127–140.